DEVELOPMENT OF MODELS FOR STRUCTURAL DEFECT CHARACTERISATION OF SELECTED METALS AND SEMICONDUCTORS BASED ON SLOW POSITRON BEAM TECHNIQUE

BY

AKPOMEDAYE, EMOGHENE ESUVBIE
(PHY/96/8946)

SUBMITTED TO

THE DEPARTMENT OF PHYSICS
FEDERAL UNIVERSITY OF TECHNOLOGY, AKURE, NIGERIA.

IN PARTIAL FULFILMENT OF THE REQUIREMENTS FOR THE AWARD OF MASTER OF TECHNOLOGY DEGREE IN SOLID STATE PHYSICS.

FEBRUARY, 2007

DEDICATION

Dedicated to my parents, Mr. and Mrs. D. E Akpomedaye, and also to my siblings Ogaga and Vos.

CERTIFICATION

We certify that this work was carried out by Mr. Akpomedaye Emoghene Esuvbie of the Department of Physics, School of Sciences, Federal University of Technology, Akure, Nigeria.

....
Dr. O. M. Osiele
B.Sc. (Ekpoma), M.Sc. (Nsukka),
PGDE (Benin), Ph.D (Akure).
(Major Supervisor)

....
Date

....
Prof. (Mrs.) I. A. Fuwape
B.Sc. M.Sc. Ph.D (Ibadan).
(Co-Supervisor)

....
Date

ACKNOWLEDGEMENT

I acknowledge my supervisor, Dr. O. M. Osiele for his painstaking supervision of my project. I acknowledge the moral and financial contributions made by my parents, Mr. and Mrs. D. E. Akpomedaye. I also acknowledge all contributions made by my colleagues in the Department towards the success of my project work. I equally acknowledge the authors of all relevant literature used in my project work.

I acknowledge the moral contributions made by my bosom friend Emeka Alaezi. I equally acknowledge the moral support of my younger brother, Ogaga Akpomedaye, and also the moral support made by my close friends and relatives towards my educational pursuit thus far.

ABSTRACT

In this work, models were developed for calculating the S parameter (amount of positron annihilation with valence electrons in low momentum regions) and W parameter (amount of positron annihilation with core electrons in high momentum regions) of materials. Experimental results obtained from Slow Positron Beam Research work for Aluminium and Silicon obtained from the Department of Physics, University of Cape Town, South Africa, were used to test the models. The models will be useful in the study of defects in materials. Moreover, the results of this work will be useful in predicting the S and W parameters, and hence defect structural characterization of materials, in studying the behaviour of positrons in materials, and also to study how defects in materials vary with any of the dependent parameters of the materials. The models were developed based on parameters such as energy of incident beam, thickness of the sample, illumination time that the S and W parameters depend on. The developed models contain some mathematical functions which were in very good agreement with experimental values. The correlation between the developed models and experimental values was calculated statistically using the Spearman's correlation. High correlation between 0.72 and 0.99 was obtained between the modeled and experimental values. The models obtained will be used as substitutes to actual experimental work in making accurate predictions of the vertical defect profile of any material.

LIST OF FIGURES

		Page
Figure 1.1:	Defect-related positron lifetime versus vacancy size of neutral vacancy clusters of silicon.	2
Figure 2.1:	Scheme of different positron experiments.	21
Figure 2.2:	Experimental positron lifetime spectra obtained in as-grown silicon.	22
Figure 2.3:	Experimental setup for the measurement of two-dimensional angular correlation of annihilation radiation using long-slit geometry.	24
Figure 2.4:	Combined perspective and contour plot of the measurement of two-dimensional angular correlation of annihilation radiation in gallium arsenide.	25
Figure 2.5:	Coincidence setup for the measurement of background-reduced Doppler-broadening spectra.	27
Figure 2.6:	Doppler-broadening coincidence spectra for zinc-doped gallium arsenide.	28
Figure 2.7:	Calculated values for the Doppler profile in aluminum.	37
Figure 2.8:	Doppler-broadening 511keV peak measured for perfect silicon.	38
Figure 2.9:	Doppler parameter S plotted as a function of positron implantation energy for GaAs substrate.	42
Figure 2.10:	Doppler-broadening 511keV peak measured for perfect silicon.	46

Figure 2.11: Doppler parameter W plotted as a function of positron implantation energy for GaAs substrate. 47

Figure 2.12: S versus W plot of positron energy scan (0-40keV) for GaAs. 49

Figure 2.13: S versus W plot of the annealing behaviour of as-grown silicon. 50

Figure 4.1: Variation of modeled and experimental S parameters with penetration depth for silicon. 57

Figure 4.2: Variation of modeled and experimental S parameters with penetration depth for aluminum. 58

Figure 4.3: Variation of modeled and experimental S parameters with implantation energy for silicon. 59

Figure 4.4: Variation of modeled and experimental S parameters with implantation energy for aluminum. 60

Figure 4.5: Variation of modeled and experimental S parameters with illumination time for silicon. 61

Figure 4.6: Variation of modeled and experimental W parameters with penetration depth for silicon. 62

Figure 4.7: Variation of modeled and experimental W parameters with penetration depth for aluminum. 63

Figure 4.8: Variation of modeled and experimental W parameters with implantation energy for silicon . 64

Figure 4.9: Variation of modeled and experimental W parameters with implantation energy for aluminium.

Figure 4.10: Variation of modeled and experimental 65
W parameters with illumination time for silicon. 66

TABLE OF CONTENT

LIBRARY * FED. UNIV. OF ...

Page

Title Page

Dedication i

Certification ii

Acknowledgement iii

Abstract iv

List of Figures v

Table of Content vii

CHAPTER ONE

INTRODUCTION

1.0 The Positron 1

1.1 Positron Sources 4

1.1.1 Radioactive Sources 4

1.1.2 Pair Production 5

1.2 Positron Moderation 6

1.2.1 Physics of moderation 6

1.2.2 Moderating materials 6

1.3 Positron Transport 7

1.4 The Positronium 8

1.5 Excitation and Scattering 9

1.6 Energy Loss and Implantation 10

1.7 Diffusion Models and Quantum Motion 11

1.8 Electron-Positron Correlation and Annihilation 12

1.9 Trapping and Detrapping 13

1.10 Surface Processes 14

1.11 Reemission and Branching 14

1.12 Interactions with Metals 15

1.13 Interactions with Semiconductors 15

1.14 Backscattering 17

1.15 Channeling and Thermalization 17

1.16 Objectives and Significance of The Study 18

CHAPTER TWO

LITERATURE REVIEW

2.1 Positron Annhihilation Spectroscopy 20

2.2 Angular Correlation Measurements 23

2.3 Annihilation Line Doppler-Broadening 26

2.4 Positron Microprobe 28

2.5 Age-Momentum Correlation 29

2.6 Positron Annihilation Induced Auger Electron Spectroscopy (PAES) 29

2.7 Low Energy Positron Diffraction 30

2.8 Positron-Induced Secondary Electron Emission 30

2.9 Positron Backscattering 31

2.10 Annihilation Lineshape Doppler Model 31

2.11 Lineshape Parameters 36

2.11.1 S parameter 37

2.11.2 W parameter 45

2.11.3 S/W parameter 48

2.12 Factors Affecting Lineshape Parameters 50

2.12.1 Temperature 50

2.12.2 Implantation energy 51

2.12.3 Energy resolution 52

2.12.4 Mean depth 52

CHAPTER THREE

METHODOLOGY

3.1 Modeling of S Parameter 53

3.2 Modeling of W Parameter 54

CHAPTER FOUR

RESULTS AND DISCUSSION

4.1 Introduction 56

4.2 Results and Discussion of S Parameter 57

4.3 Results and Discussion of W Parameter 62

CHAPTER FIVE

CONCLUSION AND RECOMMENDATION

5.1 General Conclusion 67

5.2 Applications of Results 68

5.3 Conclusion 68

5.4 Limitations of Study 69

5.5 Recommendations for Further Studies 69

CHAPTER ONE

INTRODUCTION

1.0 The Positron

The positron is the antiparticle of the electron. This means that it has the same mass and spin as the electron, but it is of opposite charge, i.e. one positive elementary charge. Furthermore, if a positron is surrounded by one or more electrons, the positron annihilates with one of the electrons and their masses are transformed into energy which is emitted as gamma-quanta, normally two or three, each of energy 511keV. The properties of these gamma-quanta, such as their energies, emission directions and time of emission, which can be measured, provide useful information about the materials in which positrons annihilate. This is the principle of Positron annihilation spectroscopy. It samples the electron density and defect distribution in the sample (Eldrup, 1995 and Wang et al., 2000).

Two other equally important positron probing techniques are Angular correlation and Doppler broadening. Krause–Rehberg and Leipner, (1999) reported that positron annihilation in matter was first studied at about 1930 by Mohorovicic. He discovered that the energy and momentum conservation during the annihilation process could be utilized to study properties of solids. The bound state of a positron and an electron is analogous to the hydrogen atom, where the proton is replaced by the positron. This electron–positron state is called the positronium (Ps). It was predicted by Mohorovicic in 1934 and observed by Deutsch in 1951.

In addition to the Angular correlation of annihilation gamma-quanta, Doppler broadening of the annihilation line and Positron lifetime spectroscopy were established as independent methods. Deutsch in the late 1960 discovered that the annihilation parameters are sensitive to lattice imperfections, as studied in face centred cubic (fcc), base centred cubic (bcc) and hexagonal close packed (hcp) lattices.

The trapping of the positron in defects is based on the formation of an attractive potential at open-volume defects such as vacancies, vacancy agglomerates and dislocations. The sensitivity range for the vacancy detection in metals starts at about one vacancy per 10^7 atoms or less. The positron lifetime increases in open-volume defects due to the lower electron density, as shown in Fig. 1.1. The density and momentum distribution of electrons participating in the annihilation result in observables to be detected in a positron experiment. The analysis of the annihilation radiation thus gives the possibility of defect detection. Clustering of vacancies as a typical defect reaction may be observed as the increase in the defect-related lifetime due to the further decrease in the electron density. Practically, all positron lifetimes for the important bulk semiconductor materials and many lifetimes for various vacancy type defects have been experimentally determined (Krause-Rehberg and Leipner 1999; Coleman 2000).

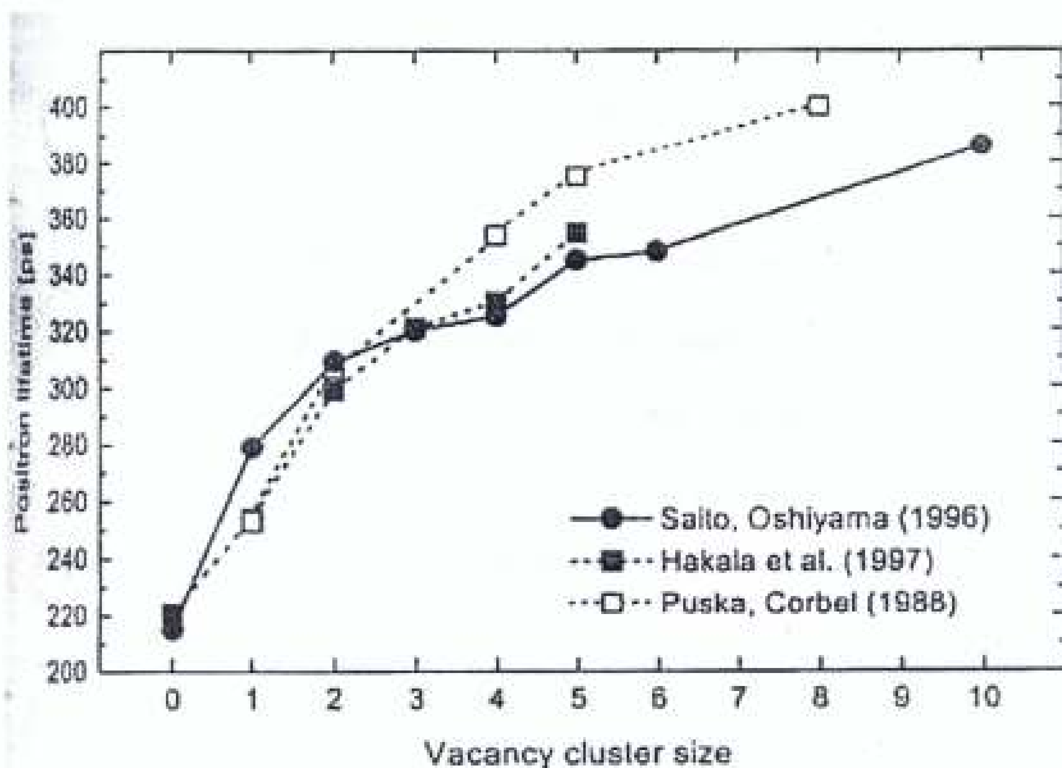

Fig. 1.1: Defect-related positron lifetime versus vacancy size of neutral vacancy clusters of silicon (Krause-Rehberg and Leipner, 1999).

In comparison with theoretical calculations, the defects can be characterized by their specific positron lifetimes. It seems to be possible to obtain chemical information on the surrounding of annihilation site by comparison of measured and theoretically calculated Doppler spectra in the high momentum region. A new development is the use of different curves of the Doppler broadening annihilation lines as fingerprints for specific annihilation sites. These curves are otherwise known as the S-, W- and H- parameters (Krause-Rehberg and Leipner, 1999).

In principle, dislocations are also positron traps in semiconductors. In addition to the positron traps known from metals, negatively charged non-open-volume defects, e.g. acceptor type impurities or negatively charged anti-sites in a compound, represent positron trapping centres at low temperatures. Positrons may be bound with a small binding energy to such centres, which are called shallow positron traps. In summary, neutral and negative vacancy type defects, as well as negative ions, are the dominant positron traps in semiconductors, hence temperature dependent lifetime measurements may distinguish between both defect types (Krause-Rehberg and Leipner, 1999).

Doppler broadening of the annihilation radiation samples the local electron momenta. Large differences in the annihilation characteristics between freely diffusing and localized positrons allow a relatively easy characterization of materials with respect to possible defects present. The position lifetime is registered as the time difference between the emissions of the 1.27MeV gamma-quantum generated almost simultaneously with the positron in a ^{22}Na, which is the most commonly used positron source, and detection of one of the 0.511MeV annihilation gamma-quanta. The two other techniques are based on the principle of the conservation of momentum in the annihilation process. The momentum distribution of the electron-positron pair is conserved in the annihilation radiation. The momentum component in the gamma-ray propagation direction leads to a small Doppler shift of the annihilation. Several million annihilation events are summed up as a Doppler broadened spectrum of the 511keV line in a

annihilation events are summed up as a Doppler broadened spectrum of the 511keV line in a spectrometer. Also, the momentum components in the other two space directions result in the deviation of the angle from collinearity of the two 511keV annihilation gamma-quanta. These setups are called one-dimensional (1-D) and two-dimensional (2-D) Angular Correlation of Annihilation Radiation (ACAR) (Krause-Rehberg and Leipner, 1999).

Due to the broad energy distribution of the positrons resulting from the β^+ decay, the penetration depth is also broadened and thus these methods are not suitable to investigate near-surface defects or for defect profiling. Rather, the slow positron beam technique uses mono-energetic positrons from moderators. The energy of such a positron beam can be set in a wide range to allow near surface defect profiling. Doppler broadening and Angular correlation measurements as well as Positron lifetime spectroscopy, can be carried out with a slow positron beam too. In addition to these, other less important techniques worthy of mention are Positron Annihilation Induced Auger Electron Spectroscopy (PAES) and Age-momentum correlation (Krause-Rehberg and Leipner, 1999).

1.1 Positron Sources

1.1.1 Radioactive sources

The choice of radioactive source for positron beam experiments is governed by the nature of the measurements, with respect to its production or availability. ^{22}Na positron source from the β^+ decay

$$^{22}{}_{11}\mathrm{Na} \longrightarrow \quad ^{22}{}_{11}\mathrm{Ne} + \beta^+ + \upsilon_e + \gamma, \qquad (1.1)$$

gives a relatively high 90.4% positron yield, and is preferred for most long term experiments, offering an acceptable cost per Becquerel and has half-life of 2.6 years due to the simple reason that the energy spectrum of positrons from ^{22}Na is peaked at 178keV and its end point is 545keV.

beta positrons if their direction is unchanged. Therefore, to create a highly polarized positron beam, it is desirable to use a low-atomic-number (Z) backing material to minimize backscattering in the source capsule, with consequent unavoidable loss of intensity. The associated gamma-ray emitted during the β^+ emission is used as a start signal in high resolution positron lifetime experiments.However, it may not be suitable for momentum distribution experiments, except backscattering is properly shielded.

Other isotopes (^{64}Cu, ^{58}Co, etc) can be used, but less frequently. In addition, positronium dissociation in high energy photons is an alternative positron source using appropriate separation fields, though this is quite expensive for common laboratory work. Its advantage is that due to the very high start signal initiated, it is fundamental to three–dimensional Angular Correlation of Annihilation Radiation (3D–ACAR) experiments (Coleman, 2000).

1.1.2 Pair production

In this case, an electron beam is stopped in an absorber of high – atomic number, such as Ta, W or Pt, creating Bremsstrahlung rays and positronium. For electron beam of sufficiently high energy, the generation probability of positronium is high, while the moderation or bunching of the fast positronium produced leads to a pulsed positron beam which can be exploited in certain experiments (Coleman, 2000).

1.2 Positron Moderation

1.2.1 Physics of moderation

Primary positrons which are not backscattered on entering a solid, rapidly lose energy by inelastic collisions, primarily with core and conduction electrons. If implanted into a metal with energy greater than a few keV, a positron will reach thermal equilibrium with its surroundings at about 40meV in 1 picosecond.

The moderation efficiency ε is the number of mono-energetic positrons delivered to a target per unit time divided by the activity of the primary positron source. The moderation efficiency ε for radioactive $^{22}{}_{11}$Na can be taken as

$$\varepsilon = y_0 L / R \tag{1.2}$$

where R is the positron mean range, y_0 is the branching ratio for positron re-emission from the surface, L is the dimension from the surface to the point of thermalization. For L = 100nm, y_0 = 0.35 and R = 15μm, $\varepsilon = 2 \times 10^{-3}$. Thus, only low-energy primary positrons (10keV) are stopped within a diffusion length of the surface, and the others annihilate deep inside the material (Coleman, 2000).

1.2.2 Moderating materials

Dale et al. (1980), demonstrated that well-annealed tungsten had moderation efficiency ε approximately 1×10^{-3}, after minimizing the concentration for non-equilibrium defects. The high workfunction of tungsten has made it the most widely used moderator material for many years, and its efficiency is not seriously reduced by exposure to air or layers of surface contamination. It can be prepared externally and transported through air for installation at the beam system, without significant moderation degradation. Both polycrystalline and single crystal tungsten have been successfully used as moderators (Coleman, 2000).

Backscattering geometries exploit the high efficiencies of well prepared metallic single crystals. The conical moderator geometry of Lynn, which for tungsten achieves a moderation efficiency as high as 1.5×10^{-3}, is technically sophisticated (in terms of annealing and positioning). Apart from the cone and reverse cone, other good geometries of 1.1×10^{-3} to 1.4×10^{-3} nm are the Venetian blind, thin film, mesh, deposited moderator, self moderator source and thin film with cone (Coleman, 2000).

1.3 Positron Transport

Positrons are transported from moderator to target by magnetic fields, electrostatic fields, or a mixture of both through reflectors, velocity filters, apertures, accelerators and lenses of various designs. To avoid having extremely long systems which rely on the inverse square law to reduce background, it is now common to use bent solenoids or electromagnetic filters to remove fast positrons from the beam and allow more efficient shielding of the positron source. Electrostatic beams are employed for beam transport, though they are more complex than magnetic transport. They have advantage over magnetic focusing in the areas of beam manipulation, reflection, focusing, hence ensuring more precise measurements.

Beam brightness is defined as the concentration of positrons of a particular energy per second per unit cross-sectional area, with a small angular divergence. To increase beam brightness, positrons are focused onto a small spot on the moderator surface and are then re-emitted normally to the surface (Coleman, 2000).

Hybrid beams are also available, which employ magnetic transport and electrostatic manipulation in the experimental setup for a range of experiments. To accelerate a beam from source, a sufficient varying negative potential is applied between the target and source. Positrons can be accelerated after passing through the velocity filter, just before they enter the experimental region. This means the whole of the source/moderator end of the system is raised to

the accelerating potential and that the target environment is at ground. Channel electron multiplier arrays (CEMA) are commonly used to obtain images of positron beams. They consist of arrays of 10μm-diameter tubes some 5000μm long, with a maximum effective ope.. area of 70%. Several spectroscopic techniques e.g. retarding field, hemispherical, cylindrical mirror, electromagnetic (E × B) analyzers have been used in positron beam lines. These devices are used after the positron has reached its target (Coleman, 2000).

1.4 The Positronium

The positronium is the bound state of a positron and an electron. The positronium can exist in either a spin state of zero or a spin state of one. When the spin of the positronium is zero, the positron and electron spins are antiparallel and the singlet is known as para-positronium (p-P_S). When the spin is 1, the triplet is known as ortho-positronium (o-Ps).

Free para-positronium decay occurs by the emission of an even number of photons, while that of ortho-positronium is via the emission of an odd number of photons. The most common decay mode of ortho-positronium is via the emission of three 511keV quanta possessing a characteristic distribution of energies, while that for para-positronium is two 511keV gamma-quanta emitted in its rest frame back-to-back. The decay rate of ground state o-Ps in vacuum has been measured more often than any other positronium property and is taken as 3.2ns, while the 125ps para–positronium ground state lifetime has been measured successfully only twice, with a 1% precision, by utilizing an ortho-positronium and para-positronium mix in a uniform magnetic field and assuming a ground state hyperfine splitting value (Coleman, 2000). The positronium ion is denoted Ps^- . It is formed from a positron together with two electrons in relative spin singlet state. Coleman,(2000) reported that its bound state was first predicted by Wheeler in 1946 and experimentally detected by Mills in 1981. The observation of the positronium ion by Mills

(1981) used a technique analogous to the production of hydrogen ion by proton bombardment of thin foils (Coleman, 2000).

1.5 Excitation and Scattering

Models for inelastic scattering can be divided into two classes. One is based on the dielectric response of the medium, which naturally emphasises the collective and delocalized nature of the excitations. The other approach is based on scattering of individual atoms in the medium. According to Linear Response Theory, the doubly-differential inelastic cross-section is proportional to the imaginary part of the inverse of the dielectric function of the medium. The formalism of the energy and momentum dependent dielectric response includes both electron-hole and plasma excitations in a natural way, with various schemes to account for electron-electron correlations in terms of so-called local field corrections. In insulators, the presence of the energy gap between the valence and conduction bands prohibits ionization and electron-hole pair creation processes when the positron has slowed down to energies equal to or smaller than the gap. Thereafter, processes which lead to the formation of excitons and positronium are possible until the positron kinetic energy is a few eV at below the gap.

The stopping power $S(E)$ of electrons and positrons at kinetic energy E is defined as the energy lost per distance traveled. It is mathematically expressed as

$$S(E) = \frac{-dE}{dx} \tag{1.3}$$

At energies above 100keV, the relativistic Mott cross-section describes elastic scattering of both electrons and positrons off the nuclei. At lower energies, the cross-section should be obtained from the true crystalline potential. For electrons, this potential includes the exchange contribution, as the scattering electron state must be orthogonal against the core states. Thus a good approximation for the electron potential in the core region is given by the self-consistent

Hartree-Fock potential. Positrons see only the electrostatic potential plus a relatively weak correlation contribution (Coleman, 2000).

1.6 Energy Loss and Implantation

Positrons implanted into a solid are assumed to rapidly lose energy to attain an initial depth distribution before diffusing back to the surface or annihilating. The approach to near thermal energies is dominated by electron scattering times for phonon dominated diffusion (Britton, 1994). In the early stages of thermalisation, the positron motion is random between collisions, and it is convenient to make implantation and diffusion calculations based on collision cross sections and Monte Carlo simulation techniques (Coleman, 2000).

The Monte Carlo methods provide accurate statistical distribution of the slowing-down positron in arbitrary geometry, with several computer codes available, offering various degrees of sophistication in the cross-sections they use for elastic and inelastic processes. With this, the Monte Carlo methods also provide detailed information of the energy and angle dependent backscattering of surfaces, as well as the spectrum of secondary electrons. As the motion ceases to be unprobable at low energies and the cross-section data becomes less accurate, the Monte Carlo simulations are usually terminated at a cutoff energy of order 10 – 50eV (Coleman, 2000).

The mean implantation range was found to be

$$Z_0 = \alpha E^{1.6/\rho}, \tag{1.4}$$

where E is the incident positron energy, ρ the density and $\alpha = 450\mu\mathrm{gcm}^{-2}$ (Britton, 1994).

Prior to full thermalization, the positrons move as epithermal particles. At low implantation energies, a substantial part of the positrons can escape from the surface before thermalization, and attempts have been made to use the epithermal part of the spectrum also in quantitative surface studies. (Coleman, 2000).

1.7 Diffusion Models and Quantum Motion

Although the quantum nature of the thermalised positron is manifest, over length scales larger than mean free path, the positron motion is best described as diffusive. The ground state wavefunction of a thermalised positron in condensed matter is that of a thermal de Broglie wave, modulated by the randomized motion due to repulsion from positive ion cores (Coleman, 2000).

In the single-group diffusion model, the evolution of the positron depth distribution is given by the one-dimensional diffusion annihilation equation

$$\frac{\partial u}{dt} = D_{\theta} \frac{\partial^2 u}{\partial Z^2} - [\lambda + \mu(Z)]u_{\theta} \ , \qquad (1.5)$$
$$P(Z,E) = u_{\theta}(Z,0)$$

at energy $E = 0$,

where $P(Z,E)$ is the implantation profile and D_{θ} is the thermal positron diffusion coefficient (Britton, 1994).

In the two-group model, epithermal positrons act as time-dependent sources of thermal positrons, with a thermalization length approximately equal to the mean free path for inelastic positron-phonon scattering. Thermal equilibrium processes can thus be separated from diffusion processes. In this model, the time development of the system is described by two-coupled diffusion annihilation equations

$$\frac{\partial u_E}{\partial t} = D_E \frac{\partial^2 u_E}{\partial Z^2} - [\lambda + \gamma_E + \mu_E(Z)]u_E \qquad (1.6)$$

$$\left.\begin{array}{l} \dfrac{\partial u_{\theta}}{\partial t} = D_{\theta} \dfrac{\partial^2 u_{\theta}}{\partial Z^2} - [\lambda + \mu_{\theta}(Z) + \gamma_{\theta}]u_{\theta} \\ \\ u_E\,(Z,0) = P(Z,E) \text{ and } u_{\theta}\,(Z,\theta) = 0 \end{array}\right\} \qquad (1.7)$$

The subscripts θ and E refer to the thermal and epithermal states respectively, λ is the bulk annihilation rate, μ is the spatially dependent trapping rate to a distribution of defects, and γ is the thermalization rate (Britton, 1994).

1.8 Electron-Positron Correlation and Annihilation

Electron-positron correlation manifests itself in the pile-up of electrons around a positron. This affects the ground state energetics of positrons. The correlation energy is an important part of the positron total energy, both inside materials and at surfaces. Secondly, the annihilation characteristics depends on the details of the positron screening cloud. Both the annihilation rate, which is proportional to the contact electron density at the positron, and the momentum distribution of the annihilation quanta are affected.

The positron ground state energetics is governed by the eigenvalue

$$E_{+} = \frac{\hbar^2}{2M_{+}} \int (d\vec{r} \left| \Delta\psi_{+}(\vec{r}) \right|^2 + d\vec{r} \left| \Delta\psi_{+}(\vec{r}) \right| V(\vec{r})) \tag{1.8}$$

where M_{+} is the positron mass. The positron potential is

$$V(\vec{r}) = \phi(\vec{r}) + \frac{\delta E_{xc}[n_{+}]}{\delta n_{+}(\vec{r})} + \frac{\delta E_{corr}[n_{+}, n_{-}]}{\delta n_{+}(\vec{r})}, \tag{1.9}$$

where the electrostatic potential is

$$\phi(\vec{r}) = \int \left(d\vec{r}' \frac{n_{nucl}(\vec{r}') - (\vec{r}') + n_{+}(\vec{r}')}{\left| \vec{r} - \vec{r}' \right|} \right) \tag{1.10}$$

The angle θ between the lines of sight of the two gamma-quanta of annihilation is

$$\theta = \frac{P_T}{M_0 C} < 20 mrad \tag{1.11}$$

where P_T is the total momentum of the gamma-quanta, C is light speed, M_0 is photon mass (Coleman, 2000).

In many cases, in particular in metals, the positron momentum is low, compared to the electron momentum. Hence a measured momentum distribution is essentially that for the electrons. Such measurements are being used to determine the electronic structure of metals and alloys.

The rate with which positrons annihilate with the surrounding electrons is given by

$$\lambda = \pi r_o^2 c \int e^-(\bar{r}) e^+(\bar{r}) d\bar{r} \ , \qquad (1.12)$$

where r_o, the classical electron radius, is given as

$$r_o = \frac{e^2}{M_0 C^2} \qquad (1.13)$$

and e^+ and e^- are the positron and total electron density at $\bar{r}$. The positron mean lifetime is a measure of the electron density sampled by the positron, in the sense that a lower electron density results in a longer positron lifetime (Eldrup, 1995).

1.9 Trapping and Detrapping

Positron trapping is a quantum-mechanical transition between a delocalized propagating state and a localized one, at an open-volume defect around a negatively charged impurity or at a surface. The capture rate is proportional to the density of defects on surface area and the proportionality constant is known as the trapping coefficient υ.

In semiconductors, the temperature dependence of the positron trapping rate gives information on the defect type and surface distribution. In semiconductors and insulators, positively charged defects effectively repel positrons, and the trapping rate is expected to be very small. On the other hand, negatively charged defects enhance the initial positron density in the defect region and increase the trapping coefficient (Coleman, 2000).

The trapping cross section can also exhibit resonances in the eV energy region for slowing down positrons. Thermal fluctuations can lead to positron detrapping. In thermal

equilibrium, the ratio between the detrapping (δ) and trapping (k) rates for point defects in three dimensions is

$$\frac{\delta}{k}=\frac{1}{C_{\upsilon}}\left[\frac{m_{*}K_{B}T}{2\pi\hbar^{2}}\right]^{3/2}\exp(-E_{b}/2KT) \tag{1.14}$$

where E_b is the positron binding energy to the trap and C_{υ} the defect concentration (Coleman, 2000).

1.10 Surface Processes

A useful application of positron beams is the study of defects below the surface or at buried surfaces. The signal is observed either through the arrival and subsequent annihilation of positrons reaching back at the outer surface after initial implantation, or through the direct annihilation signals of positrons being consumed below the surface. For the latter, momentum distribution measurements usually based on the Doppler broadening techniques is used, although lifetime measurements with time-structured beams are now also feasible. Typical backscattering probability in the energy range of 100eV is 10^{-3}. The elastic scattering events resulting in the diffraction take place in time scales of 10^{-6}s, before appreciable inelastic collisions take place (Coleman, 2000).

1.11 Reemission and Branching

Assuming free-electron like dispersion relations near the surface and smooth matrix elements coupling the initial and final states, one can make simple estimates of the branching ratio between positron and positronium emission rates. This is basically a density-of-states argument, which leads to the positronium-positron branching ratio

$$\frac{\Lambda p_{s}}{\Lambda e^{+}}\propto A\frac{/\phi_{p_{s}}/^{3/2}}{/\phi_{+}/^{1/2}} \tag{1.15}$$

where ϕ_{p_s}, ϕ_{+} are Ps and e^{+} workfunctions respectively,

and the slow positron yield as a function of ϕ_+ is

$$y = \frac{\sqrt{|\phi_+|}}{\sqrt{|\phi_+|+b}} \tag{1.16}$$

where b is a constant.

An alternative picture of the branching ratio uses time-dependent non-equilibrium perturbation theory to obtain the slow positron yield as

$$y = A\exp\left[-\sqrt{\frac{\phi_0}{\phi_+}}\right] \tag{1.17}$$

where ϕ_0 is a constant characteristic of the metal in question (Coleman, 2000).

1.12 Interactions with Metals

In a perfect metal lattice, the positron will, after slowing down, diffuse around, normally in a delocalized, Bloch-function state. Positron lifetimes in metals are 100 to 400psec, depending upon the metal. During its lifetime, the positron typically diffuses about 200nm. Furthermore, the average conduction electron momentum at a defect is lower than in the bulk, and the positron overlaps less with the high momentum core electrons. Both these defects lead to a narrower total momentum distribution for the annihilation quanta. These changes in annihilation characteristics for defect-trapped positrons are the basis for the now well established use of Positron annihilation spectroscopy for metal defect studies. It should be noted in particular that interstitials or small clusters of these do not trap positrons. Thus the positron is specifically sensitive to vacancy-type defects in low density regions. For positrons trapped in vacancy clusters, their lifetime will generally increase with cluster size (Eldrup, 1995).

1.13 Interactions with Semiconductors

Positron lifetimes in perfect bulk semiconductors are of the same range as that for metals. However, the defect population in semiconductors is more complex than in metals, due to the

fact that defects may exist in different, non-equivalent lattice sites. In semiconductors, there is much experimental evidence that the characteristics of positron trapping into vacancy defects vary considerably between different semiconductors and with the position of the Fermi level in a given semiconductor (Puska et al., 1990).

Positron trapping in semiconductors is to some extent analogous to the capture of free carriers at defect centers. In order that vacancy-type defects be seen in positron lifetime experiments, a positron has to reach its ground state in the defect which is a rather localized state separated from the possible Rydberg states. This implies that each state in the trapping process has to be faster than the relevant positron annihilation rate ($\approx 10^{10}s^{-1}$) in the final trapped state (Puska et al., 1990).

For both metals and semiconductors, the trapping rate is relatively equivalent, and is given by

$$K = \frac{2\pi}{\hbar} \sum_{i,f} p_i M_{if}{}^2 \delta(E_i - E_f), \tag{1.18}$$

where p_i is the occupation probability of the initial state, M_{if} is the transition matrix element between the initial and final states, E_i and E_f are the respective energies. For transition-limited trapping, $K_{tl} = \mu C$, and for diffusion-limited trapping, $K_{dl} = 4\pi r_d D_+ C$. C is the defect concentration, μ is the positron trapping coefficient, r_d is the defect radius while D_+ is the positron diffusion parameter. In general, the positron trapping rate is given as the superposition of transition- and diffusion-limited trapping, and is expressed as

$$\frac{1}{K} = \frac{1}{K_{tl}} + \frac{1}{K_{dl}} \tag{1.19}$$

(Krause-Rehberg and Leipner, 1999).

1.14 Backscattering

Depending on the incident energy of the positrons and on the sample material, there is a certain probability for the backscattering of highly energetic positrons from the sample. The backscattering probability was treated theoretically by Monte Carlo simulations, taking into account both elastic and inelastic scattering for Al, Au, Si and Ge (Krause-Rehberg and Leipner, 1999). A high–atomic number target leads to high backscattering. Backscattering positrons annihilate outside the sample, leading to spectral distortion. Otherwise, some of the backscattering positrons may reach accelerator stage and reaccelerate back into the sample. Use of (i) shielding of annihilation radiation detector (ii) large specimen chamber and (iii) large separation between specimen and accelerator, help to reduce measurement errors in spectrum experiments.

1.15 Channeling and Thermalization

The prerequisite for positron channeling is a beam with very low divergence. This is not the case for magnetically transported beams used for defect studies. Channeling is of minor importance in defect profiling.

Thermalization is shorter than total positron lifetime. The energy transfer rate is very high at large energies and proceeds by core ionization processes. This means that positron energy is decreased rapidly. The dominant process in semiconductors is the excitation of electron-hole pairs for energies higher than the bandgap width (Krause-Rehberg and Leipner, 1999).

When the positron reaches thermal energies, they start to diffuse through the lattice and behave as charged particles. The positron diffusion can be described similarly to electrons with the semi-classical three-dimensional Random Walk Theory. The positron diffusion length L_+ is limited due to the finite lifetime of positrons in the defect-free bulk, γ_b. It is expressed mathematically as

$$L_+ = \sqrt{\gamma_b D_+},\ D_+ = \frac{\gamma_r K_B T}{m^*} \qquad (1.20)$$

where γ_r is the scattering relaxation time, m^* is the effective mass of the positron, K_B is the Boltzmann constant, T is the temperature.

The positron diffusion can be influenced by the presence of electric fields. Britton et al. (1994) demonstrated the influence of electric fields on positron diffusion in a combinational n-doped layer buried in intrinsic Si, and laid over a p-substrate. The presence of crystal defects and electric fields influences the effective diffusion length L_{eff} by

$$L_{eff} = \frac{1}{\sqrt{\frac{\lambda_{eff}}{D_+} + \left(\frac{eE_{drift}}{2K_B T}\right)^2} - \frac{e|E_{drift}|}{2K_B T}} \qquad (1.21)$$

The positron mobility is

$$\mu_+ = \frac{eD_+}{K_B T} \qquad (1.22)$$

The effective diffusion length increases with the drift electric field strength E_{drift}. The number of positrons diffusing back to the surface in the positron experiment is higher or lower, depending on the sign of the drift electric field (Krause-Rehberg and Leipner, 1999).

1.16 Objective and Significance of The Study

The scopes of this research are as follows:

(i.) Models were developed for the calculation of the S and W parameters of metals and semiconductor materials.

(ii.) Experimental results obtained from Slow Positron Beam Research work for aluminum and silicon obtained from the Department of Physics, University of Cape Town, South Africa , were used to test the models.

(iii.) The models were used to study defects in these metals and semiconductor materials.

The specific objectives are to:

(a) Develop models for the calculation of positron annihilation with valence electrons (S-parameter) and core electrons (W-parameter) for some selected metals and semiconductors; and

(b) Use the developed models to calculate and predict the S- and W-parameters of the selected materials for comparing the obtained results with experimental values.

The significance of study:

(i) The study is expected to provide models for the calculation and analysis of the variation of S- and W-parameters of metals and semiconductors with penetration depth of positrons and positron implantation energy of metals and semiconductors,

(ii) Structurally characterize them using the developed models, and

(iii) The study is expected to provide models for characterising materials structurally.

CHAPTER TWO

LITERATURE REVIEW

2.1 Positron Annihilation Spectroscopy

In some materials, the workfunction for positrons at the surface is negative, as a consequence of a relatively low electron-positron correlation force. The workfunction ϕ_+ can be separated into.

$$\phi_+ = -D - E_0 - E_{corr} \tag{2.1}$$

where D is the potential barrier due to the surface-dipole layer which acts to repel the positrons from the surface, E_0 is the zero point energy of the positron in the lattice, E_{corr} is the correlation energy of the positron in the electron gas. A negative workfunction means that any positron that enters the material and diffuses back to the surface before annihilation may be reemitted back with a mean energy corresponding to the workfunction.

After a positron has been injected into a solid and has thermalized, it will in most cases annihilate with the emission of two gamma-quanta, each of energy 0.511MeV. Deviations from an angle of pi radians are due to deviations from zero of the total electron-positron momentum. By measuring the angle θ, the distribution of the total momentum of the annihilating particles may be determined. In metals and semiconductors, the positron measurements therefore determine the electron momentum (Eldrup and Singh, 1997). Fig. 2.1 shows the various techniques for positron annihilation studies.

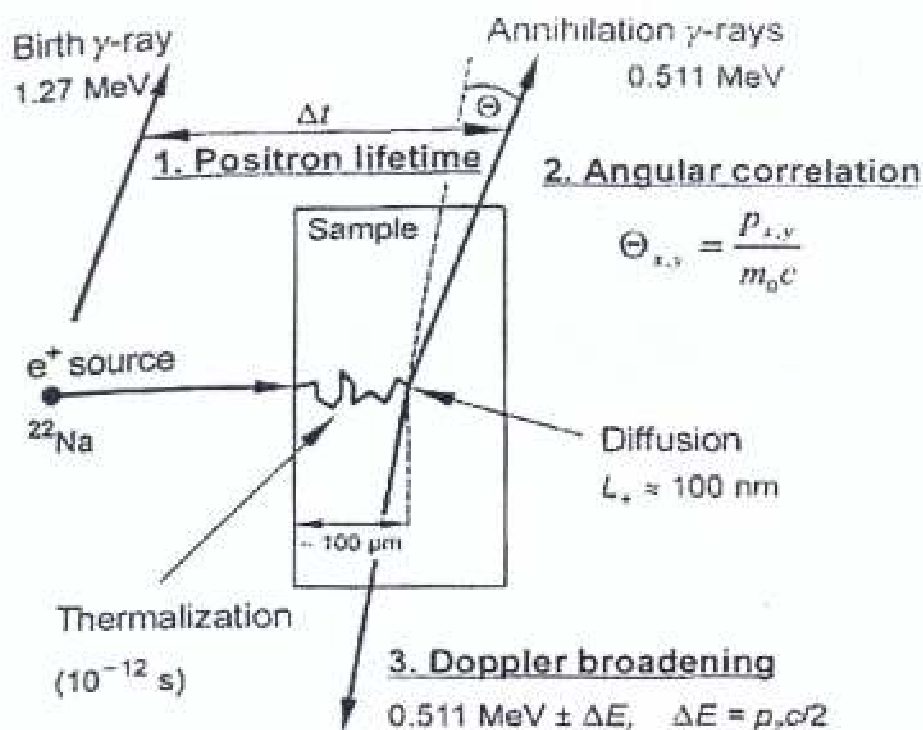

Fig. 2.1: Scheme of different positron experiments. Positrons from an isotope source (e.g. ^{22}Na) penetrate the sample, thermalise within a few picoseconds, and diffuse before annihilation (Krause-Rehberg and Leipner, 1999).

In a perfect metal lattice, the injected positrons will, after thermalization, diffuse 100 – 200nm during their lifetime. This lifetime of 100 to 400ps depends on the metal. If the metal contains defects such as vacancies, vacancy clusters, and dislocations, positrons may become trapped at these defects. When a positron is trapped in such a defect, the positron will experience a lower electron density than in the bulk material and its lifetime will increase. A typical positron lifetime spectrum is shown in Fig. 2.2.

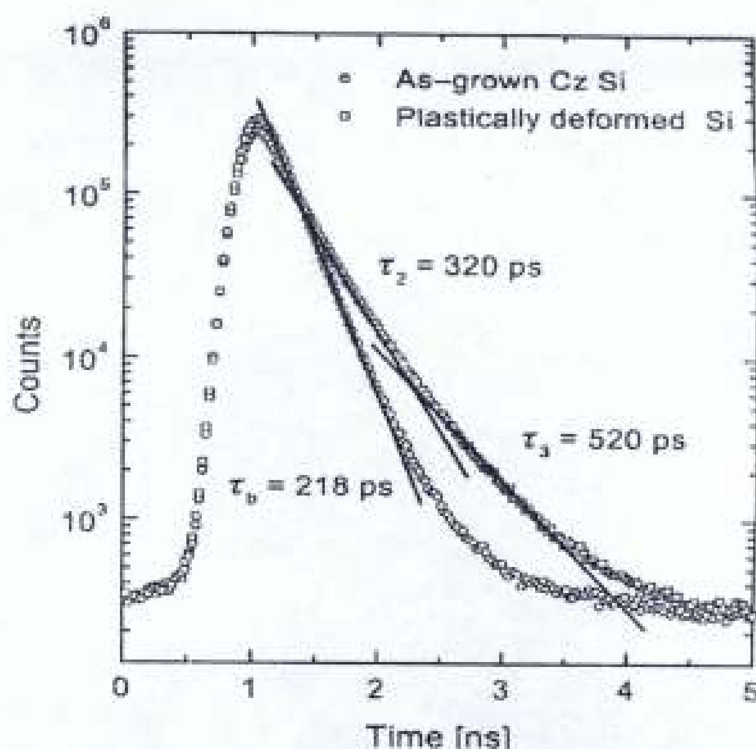

Fig. 2.2: Experimental positron lifetime spectra obtained in as-grown silicon (Krause-Rehberg and Leipner, 1999).

For larger, three-dimensional vacancy clusters, the positron lifetime approaches 500ps. However, for small clusters, if the void contains gas atoms, the lifetime will reduce (Eldrup and Singh, 1997).

The source is often made by dropping a droplet of a $^{22}NaCl$ aqueous solution on a thin foil (1mg/cm^2) or directly on the sample. Typical source strengths are 1 to 50μCi. The source is then sandwiched between two pieces of the sample, which are thick enough to ensure that all positrons are stopped in the sample. One of the two detectors signals the emission of the positron while the other detector signals the disappearance of the positron. The time difference between the two detector signals, i.e. the positron lifetime, is measured by the time-to-amplitude converter, and this is stored in the multichannel analyzer (MCA). Typically, 10^6 to 10^7 annihilating positrons are recorded and the MCA produces a histogram showing the distribution

of positron lifetimes, normally referred to as the lifetime spectrum (Eldrup, 1995; Krause-Rehberg and Leipner, 1999).

The time dependent positron decay spectrum $D(t)$ in the sample is given by

$$D(t) = \sum_{i=1}^{k+1} I_i \exp\left(\frac{-t}{\tau_i}\right) \tag{2.2}$$

with k different defect types contributing to the positron trapping and related to $k+1$ components in the spectra with the individual lifetimes τ_i and intensity I_i. If no positron traps are present, the decay spectrum is reduced to

$$D(t) = \exp\left(\frac{-t}{\tau_b}\right) \tag{2.3}$$

which is the positron lifetime in the defect free bulk. The positron lifetime spectrum is the absolute value of the time derivative of the positron decay spectrum $D(t)$, and is given by

$$N(t) = \frac{D(t)}{\tau_i} = \sum_{i=1}^{k+1} \frac{I_i}{\tau_i} \exp\left(\frac{-t}{\tau_i}\right) \tag{2.4}$$

(Krause–Rehberg and Leipner, 1999).

2.2 Angular Correlation Measurements

The source is placed outside the visual field of the detectors. It shines positrons down on the sample. The directions of the two emitted photons are defined by collimators which are narrow slits in lead blocks. The sample-to-detector distance is a couple of metres, and practical angular resolutions will be 0.5 to 1 mrad. Because of this large distance, annihilation quanta from only a small solid angle are detected. In order to minimize the reduction of the counting rate due to the distance of several mm between the sample and source, a strong magnetic field of 1 tesla is usually applied to guide the positrons to the sample (Eldrup, 1995). One of the detectors (including the collimator) is fixed, while the other one can move up to cover angles θ in the

range of about -30mrad to 30mrad, as shown in Fig. 2.3. Suitable electronics count the number of pairs of 511keV annihilation quanta as a function of the angle θ.

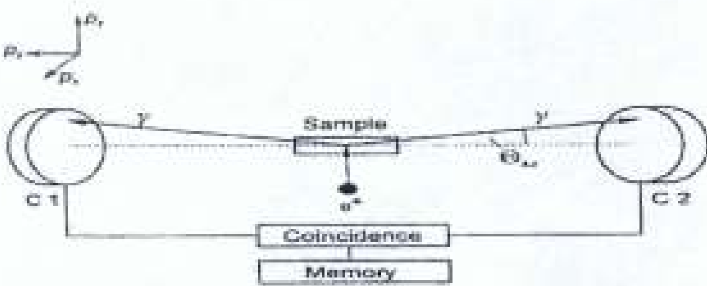

Fig. 2.3: Experimental setup for the measurement of two-dimensional angular correlation of annihilation radiation using long-slit geometry (Krause–Rehberg and Leipner, 1999).

The data are stored in the data collection unit which is often a computer that also controls the measurement. The main application of ACAR is the study of the electron structure of the bulk and defects. Two-dimensional ACAR is favourable for comparing with theoretical calculations. The momentum distribution for angular correlation of annihilation radiation in gallium arsenide is shown in Fig. 2.4.

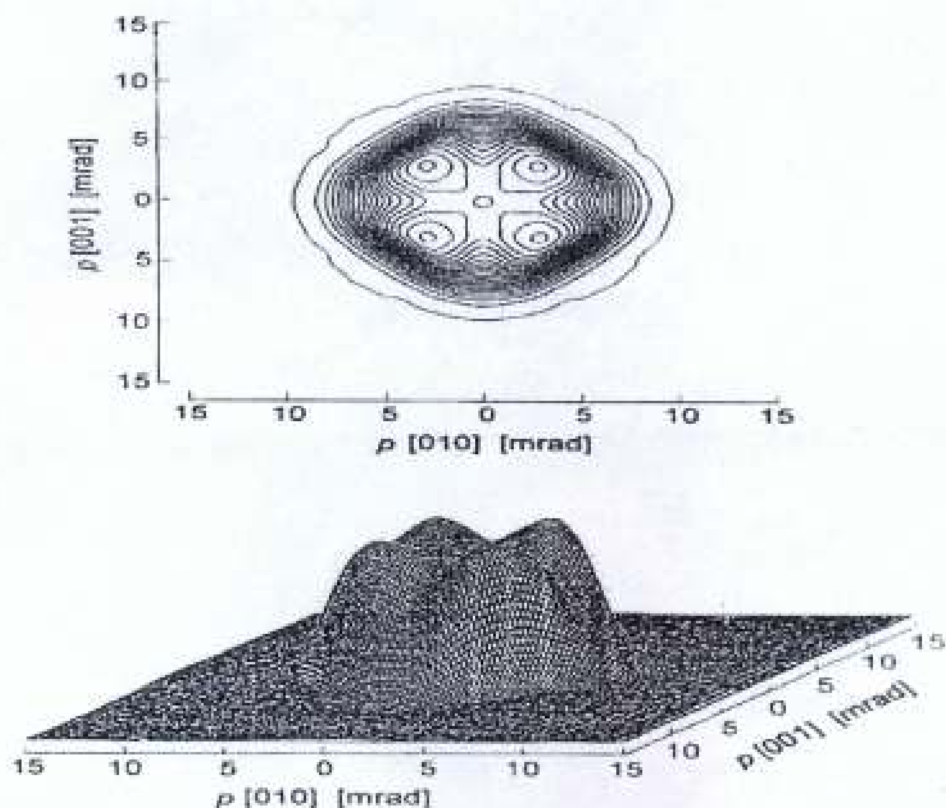

Fig. 2.4: Combined perspective and contour plot of the measurement of two-dimensional angular correlation annihilation radiation in gallium arsenide (Krause–Rehberg and Leipner, 1999).

In principle, the line shape S, W and peak H parameters can be used for ACAR. However, such a parameterization as broadly applied for Doppler broadening spectroscopy is unusual for two–dimensional ACAR, as the details of the electron structure are almost lost. To obtain defect-specific plots, a normalization for saturated positron trapping, which is for capture of all positrons in defects is necessary. This can be done by correlated positron lifetime measurements, which provide the fraction of the positrons trapped in the defect (Eldrup, 1995; Krause–Rehberg and Leipner, 1999).

2.3 Annihilation Line Doppler Broadening

The energy broadening of the annihilation line described above is measured by a high resolution energy dispersive detector system. Liquid-nitrogen-cooled pure Ge crystals of high efficiency (about 20%) are used. Under the applied high voltage of several keV, the annihilation photons cause a charge separation that is converted by a preamplifier into an electrical pulse. Its amplitude is a measure of the photon energy and can be registered after main amplification in a multi-channel analyzer (MCA). A digital peak-stabilizing system as part of the MCA allows the long-term collection of several million counts. The time of the measurements is comparable to the collection time of a positron lifetime spectrum. Both techniques can easily be performed at the same time because the Ge detector should be separated sufficiently from the sample in order to avoid pile-up effects in the detector system. If the momentum of the annihilating pair has a component P_x in the direction of the emitted gamma-quanta, the frequencies of these quanta, and hence their energies will be Doppler shifted. The energy shift is

$$\Delta E = \frac{CP_x}{2} \tag{2.5}$$

with one quantum having energy $E_0 + \Delta E$, the other $E_0 - \Delta E$, where $E_0 = mc^2 = 511\text{keV}$. By measuring the distribution of change in energy ΔE, one obtains the distribution of one component of the momentum, just like one-dimensional ACAR. Such a measurement can be done with a solid state detector of pure or compound Ge of 1.0keV Full Width at Half Maximum (FWHM) at 0.511MeV, as shown in Fig. 2.5. The signal from the detector is amplified and recorded by the multi – channel analyzer (MCA) (Eldrup, 1995).

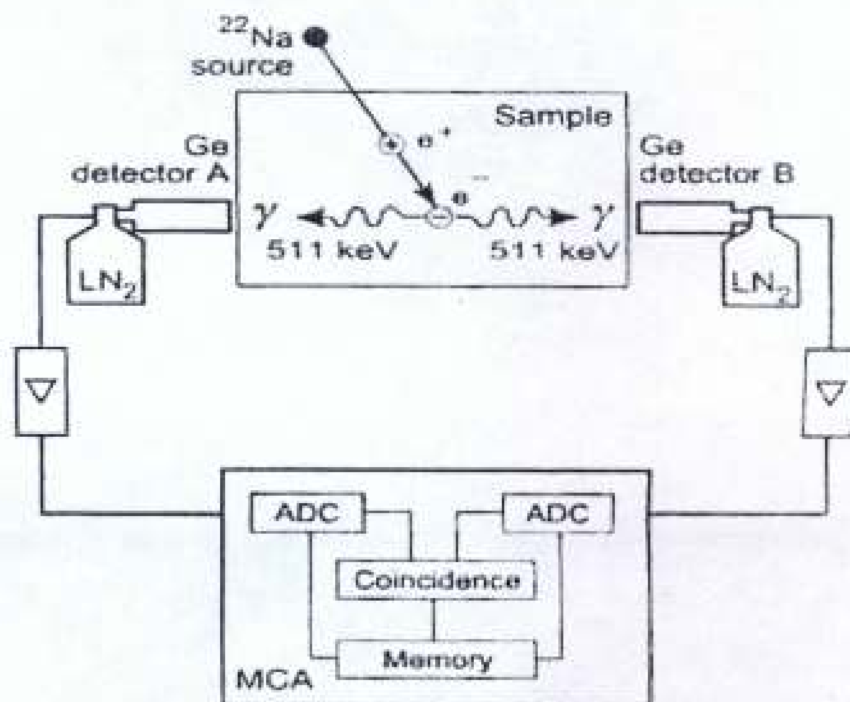

Fig. 2.5: Coincidence setup for the measurement of background-reduced Doppler-broadening spectra (Krause–Rehberg and Leipner, 1999).

The slow variable mono-energetic positron beam for Doppler broadening measurements is composed of a ^{22}Na positron source (about 50μCi) and a single tungsten 1μm foil. A fraction of the tungsten-moderated positrons, after emission from the ^{22}Na source is thermalized through a variety of collision processes and are reemitted from this moderator as mono-energetic slow positrons. The intensity of the slow positron beam is about 1.0 x 10^5 e^+/s. The incident positron energy is variable from 0 to 13keV. The measurements of Doppler–broadening spectra by slow positron beams were carried out at the room temperature by the Ge detector. The total counts in a spectrum corresponding to each incident positron energy were 8.0x10^5 e^+ /s (Sato et al., 1999; Borner et al., 1999). The Doppler broadening coincidence spectra for zinc-doped gallium arsenide is shown in Fig. 2.6.

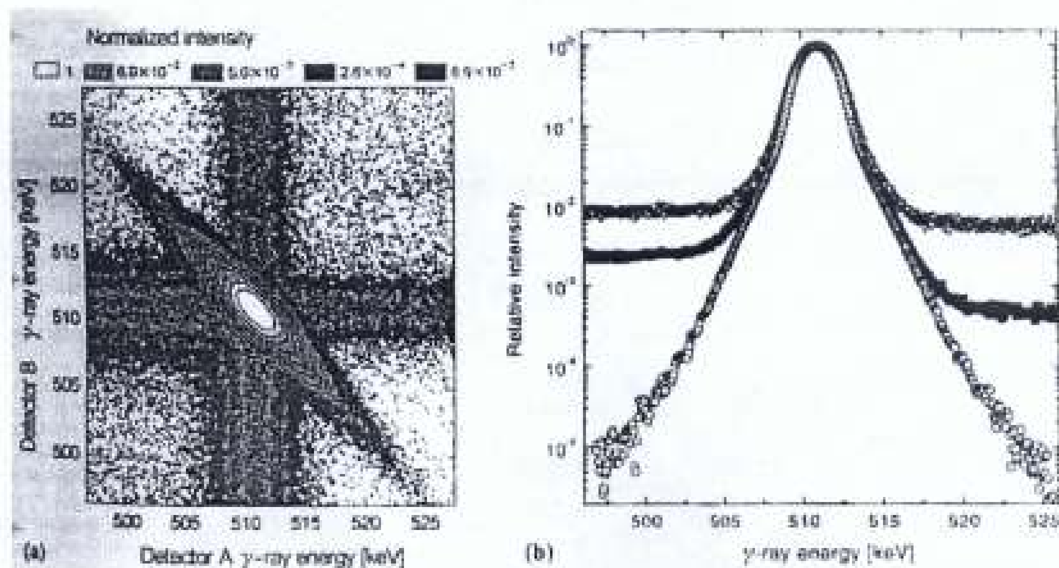

Fig.2.6: Doppler-broadening coincidence spectra for zinc-doped gallium arsenide (Krause–Rehberg and Leipner, 1999).

The result is a two-dimensional array of counting rates, where the dimensions represent the energy scalar of the respective detectors. A coincidence spectrum of both Ge detectors is obtained as the intensity profile along the diagonal from the upper left to the lower right of the measured array. The increase in the annihilation gamma-ray energy in one detector according to the Doppler shift leads to a simultaneous reduction of the gamma-ray energy in the second detector, i.e the sum of the annihilation gamma-ray energies remain constant at 1.022MeV (Krause–Rehberg and Leipner, 1999; Eichler et al., 1999).

2.4 Positron Microprobe

The transmission positron microprobe has a variety of new applications compared with transmission electron microscopy. The reduced small-angle scattering of positrons is governed by the much more effective screening of the nuclei. A strongly atomic number dependent difference in the amplitude contrast exists between electron and positron microscopy (Krause-Rehberg and Leipner, 1999).

In addition to reemission, other annihilation parameters, for example Doppler-broadening S parameter or the positron lifetime, can be detected with the help of the positron microprobe. The most important principle is the brightness enhancement of the beam using successive stages of moderation. Due to the limitation in the primary positron flux due to successive moderation stages, collimation is not practical for obtaining a micron beam spot. The brightness of a positron beam can be increased when a beam of fast positrons (≈5keV) is slowed down in a target and re-emitted as slow positrons (Stoeffl et al., 1999).

2.5 Age Momentum Correlation

The Age-momentum correlation technique combines positron lifetime spectroscopy with Doppler-broadening spectroscopy using the same annihilation event. Such a measurement is based on the registration of the collinear gamma-quanta for the positron lifetime as the stop signal and simultaneously for the measurement of the Doppler broadening of the annihilation line.

The start signal may be provided from a scintillator which must not be arranged in line with the stop detector. The positron lifetime stop signal is measured in a fast-fast spectrometer and registered in coincidence with the Doppler signal and stored in a two-dimensional memory array. The main applications of Age-momentum correlation are in positronium chemistry (Krause-Rehberg and Leipner, 1999).

2.6 Positron Annihilation Induced Auger Electron Spectroscopy (PAES)

This requires a positron beam to target low-energy positrons incident onto a surface, an electron energy analyzer for measuring the spectra of annihilation induced Auger spectra and a surface preparation and analysis chamber which can be maintained under ultra-high vacuum conditions. To date, most Positron Annihilation Induced Auger Electron Spectroscopy

measurements have been made using a magnetically guided positron beam system equipped with an energy analyzer.

The technique makes use of a fundamentally new method for the excitation of Auger electron emission in which a beam of low energy positrons is used to create the necessary core-hole excitations by matter-antimatter annihilation. The Auger process is a non-radioactive transition of electrons, where an electron from the outer shell replaces a delocalized inner-shell electron. The released energy is transferred simultaneously to another electron, known as the Auger electron. The energy levels of elements are known, and thus the analysis of the energy of the Auger electron leaving the sample provides a means of chemical analysis. The mean free path until inelastic scattering of the emitted electron is in the range of several nanometers (Coleman, 2000).

2.7 Low Energy Positron Diffraction

Low Energy Positron Diffraction relies on measurements of the diffraction of elastically scattered particles from ordered surfaces to obtain information on the arrangement of atoms in the first few atomic layers. A monoenergetic beam of particles is scattered from the sample. If the surface is well ordered, the elastically scattered particles are diffracted into directions determined from constructive interference of the scattered particle wave. Typically, the incident beam is well collimated and circular in cross-section, resulting in a set of cylindrical diffracted beams which when imaged, result in a pattern of diffracted spots (Coleman, 2000).

2.8 Positron-Induced Secondary Electron Emission

Positron-induced secondary electron emission has been used to tag or time slow positrons, in positron lifetime spectroscopy measurements. It is also essential to the detection of positrons by electron multiplier devices. Recent work on positron-induced secondary electron emission has focused on the electron energy spectra. Experiments of this type have been performed using the

recently completed high resolution Positron Annihilation Induced Auger Electron Spectroscopy system at University of Texas at Arlington, USA and University of East Anglia, UK.

Epithermal positron emission from solid surfaces can have significant effects on the interpretation of experimental data involving the recording of an annihilation lineshape parameter as a function of implementation energy such as those collected in defect profile measurements. It is likely that epithermally reemitted positrons are present in the electron-induced spectrum at low energies, but it is impossible to separate them from the secondary electron contribution (Coleman, 2000).

2.9 Positron Backscattering

When a beam of energetic positrons impinges on a solid surface, some of the incident particles will undergo a small number of large-angle collisions and leave the target with a fraction of their original energy. These are termed backscattered positrons.

The first positron backscattering measurements were performed for the entire beta spectrum of energies from 0 to 540keV for ^{22}Na(RI). By measuring the annihilation γ-count rate from the sample target, one is essentially measuring ($1-\Omega_+$) directly, where Ω_+ is the total backscattering coefficient, and as long as the total count rate is known for the incident beam. This method was employed by Baker et al. (1988), who measured total backscattering coefficients for monoenergetic positrons incident on Al, Cu, Ag, and W targets at energies between 0.5 and 30keV (Coleman, 2000).

2.10 Annihilation Lineshape Doppler Model

The workfunction ϕ_+ for a positron is defined as the energy required to remove the positron from a material is

$$\phi_+ = -\Delta - \mu_+ \tag{2.6}$$

where Δ and μ_+ are the surface dipole potential and bulk chemical potential respectively, and they depend on their reference energy levels. The affinity associated with energy referencing can be avoided by utilizing the electron workfunction

$$\phi_+ = \Delta - \mu_- \tag{2.7}$$

from which we obtain

$$\phi_+ = -A_+ - \phi_- \tag{2.8}$$

Also,

$$\phi_- = \chi + E_g \tag{2.9}$$

where χ is the electron affinity and E_g is the band gap. ϕ_- is obtained experimentally, while A_+, the positron affinity, is obtained from theoretical calculations (Berling et al., 1999).

The one-dimensional diffusion model of positrons is

$$\left.\begin{aligned} D_+ \frac{d^2 n(z)}{dz^2} - \lambda_{eff}\, n(z) + p(z,E) = 0 \\ p(z,E) = \frac{z^{-1}}{z_0} \exp\left[-\left(\frac{z}{z_0}\right)^m\right] \end{aligned}\right\} \tag{2.10}$$

(Uedono et al., 2000; Gramsch et al., 1999; Krause-Rehberg and Leipner, 1999).

or as given by Baker et al. 1991,

$$p(z,E) = \frac{-d}{dz}\left[\exp\left(\frac{-z}{z_0}\left(1 + \frac{z}{z_0}\right)^2\right) m\right] \tag{2.11}$$

where D_+ is the positron diffusion coefficient, $n(z)$ is the positron probability density at mean depth z which is proportional to z_0 by

$$z_0 = z / \Gamma\,[(1/m) + 1] \tag{2.12}$$

and Γ is a gamma function, λ_{eff} is the positron escape rate, and $p(z,E)$ is the positron implantation profile,

$$\bar{z} = AE^{n} = \alpha E^{m} \ , \qquad (2.13)$$

where A is a constant equal to thickness of thin film, n is a dimensionless constant, m is the shape parameter of $p(z, E)$, and is approximately 2. (Coleman, 2000).

The mean depth of implantation z is given by

$$z = AE = \alpha E^{1.6/\rho} , \qquad (2.14)$$

where $A = \alpha = 450\mu gcm^{-2}$, E is the incident positron energy, $n = 1.6/\rho = 1.5$, where ρ is the electron density of the sample. (Gramsch et al., 1999; Coleman and Britton, 1994).

The one-dimensional diffusion annihilation equation is

$$\frac{\partial u_\theta}{\partial t} = D_\theta \frac{\partial^2 U_\theta}{\partial z^2} - [\lambda + N(z)]U_\theta \qquad (2.15)$$

while the two-coupled diffusion annihilation equation is

$$\left.\begin{aligned} \frac{\partial u_E}{\partial t} &= D_E \frac{\partial^2 U_E}{\partial z^2} - [\lambda + \gamma_E + N_E(z)]U_E \\ \frac{\partial U_\theta}{\partial t} &= D_\theta \frac{\partial^2 U_\theta}{\partial z^2} - [\lambda + N_\theta(z) + \gamma_\theta]U_\theta \end{aligned}\right\} \qquad (2.16)$$

where

$$\left.\begin{aligned} U_E(z,0) &= p(z,E) \\ U_\theta(z,\theta) &= 0 \end{aligned}\right\} \qquad (2.17)$$

The subscripts θ and E refer to the thermal and epithermal states respectively, D_θ and D_E are the thermal and epithermal diffusion coefficients respectively, λ the bulk annihilation rate, N is the spatially dependent trapping rate to a distribution of defects, and γ is the thermalization rate (Britton, 1994).

The relationship between the diffusion length L_+ and λ_{eff} is given by

$$L_+ = \frac{1}{\sqrt{\frac{\lambda_{eff}}{D_+}}} \tag{2.18}$$

But the presence of defects and electric fields influence the diffusion length by

$$L_{eff} = \frac{1}{\sqrt{\left(\frac{\lambda_{eff}}{D_+}\right)+\left(\frac{eE_{drift}}{2k_BT}\right)^2-\left(\frac{eE_{drift}}{2k_BT}\right)}} \tag{2.19}$$

and hence, the positron mobility is given by

$$N_+ = \frac{eD_+}{k_BT} \tag{2.20}$$

where e is the electronic charge, E_{drift} is the positron drift electric field, k_B is Boltzmann's constant and T is the sample temperature. The positron decay spectrum is given as a sum of several Gaussian profiles, and is given as

$$D_f(t) = \sum_{i=1}^{k+1} \frac{I_i}{2} \exp \frac{\left[-(t-t_0)-\left(\tau_s^2/4\tau_i\right)\right]}{\tau_i} \left[1 - erf\left(\frac{1}{2\tau_s\tau_i} - \frac{t-t_0}{\tau_s}\right)\right] \tag{2.21}$$

where I_i is the individual positron intensities, τ_i is the individual positron lifetimes, $(t-t_0)$ is the measurement period at energy resolution, τ_s is a standard deviation of positron lifetimes, and k is the number of defect types contributing to $k+1$ components in the averaged spectra. If no positron traps are present, the decay spectrum reduces to

$$D(t) = \exp\left(-t/\tau_b\right) \tag{2.22}$$

where τ_b is the positron lifetime in the bulk and is equal to $\frac{1}{\sqrt{\lambda_i}}$, λ_i is the positron annihilation rate (Krause-Rehberg and Leipner, 1999).

The rate with which positrons annihilate with the surrounding electrons is given as

$$\lambda = \pi r_0^2 c \int e^-\left(\bar{r}\right) e^+\left(\bar{r}\right) d\bar{r} \tag{2.23}$$

where r_0 is the classical electron radius

$$r_0 = \left(e^2 / m_0 c^2 \right) \quad (2.24)$$

e^- and e^+ are the total electron and positron densities respectively at $\bar{r}$, while c is a constant related to the positron mobility at $\bar{r}$ (Eldrup, 1995; Krause-Rehberg and Leipner, 1999; Coleman, 2000).

The fraction of epithermal positrons at the surface is given by

$$F_{ep}(E) = \int p(z, E) \exp\left(-z/L_{ep}\right) dz \quad (2.25)$$

where the epithermal emission arises due to elastic scattering within the scattering length L_{ep} (Uedono et al., 2000)

For both metals and semiconductors, the trapping rate is relatively equivalent to

$$K = \frac{2\pi}{\hbar} \sum_{i,f} P_i M^2_{if} \partial\left(E_i - E_f\right) \quad (2.26)$$

and is related to both the translational- and diffusion-limited trapping by

$$\frac{1}{k} = \frac{1}{k_{tl}} + \frac{1}{k_{dl}} \quad (2.27)$$

and are given by

$$\left. \begin{aligned} k_{tl} &= NC \\ k_{dl} &= 4\pi r_d D_+ C \end{aligned} \right\} \quad (2.28)$$

where P_i is the occupational probability of initial state, M_{if} is the translational matrix element between initial and final states, E_i and E_f are the respective state energies, C is the defect concentration, D_+ is the positron diffusion coefficient, N is the positron trapping coefficient, r_d is the defect radius (Krause-Rehberg and Leipner, 1999).

The position lifetime spectrum is given by

$$I(t) = \sum_{i=1}^{n} \lambda_i \, I_i \, \exp(-\lambda_i t) \tag{2.29}$$

I_i is intensity, λ_i is annihilation rate (Uedono et al., 1999; Uedono et al., 1997).

In thermal equilibrium, the ratio between the detrapping (δ) and trapping (k) rates for point defects is

$$\frac{\partial}{k} = \frac{1}{C_v} \left(\frac{m_+ k_B T}{2\pi\hbar^2} \right)^{3/2} \exp(-E_b / 2k_B T) \tag{2.30}$$

where E_b is the binding energy to the trap, while C_v is the defect concentration (Coleman, 2000; Krause-Rehberg and Leipner, 1999; Puska et al., 1990).

The model for a branching ratio Ps/e^+ is given by

$$\frac{\wedge_{Ps}}{\wedge_{e^+}} \propto \frac{|\ \varphi_{Ps}\ |^{3/2}}{|\ \varphi_+ \ |^{1/2}} \tag{2.31}$$

and the slow positron yield as a function of φ_+ is

$$y = \frac{\sqrt{|\ \varphi_+\ |}}{\sqrt{|\ \varphi_+\ | + b}} = A \exp\left[-\sqrt{\varphi_0 / \varphi_+} \right] \tag{2.32}$$

where A is a constant, $\frac{\wedge_{Ps}}{\wedge_{e^+}}$ is the branching fraction, φ_{Ps} and φ_+ are the Ps and e^+ kinetic energies, while φ_0 and b are constants to be determined experimentally. (Coleman, 2000).

2.11 Lineshape Parameters

The Doppler spectrum is obtained by integrating the total momentum density along two directions (p_x, p_y).

$$P(p_z) = \iint e(p) dp_x dp_y \tag{2.33}$$

where p_x and p_y are the directions of the annihilation gamma-quanta, which make up the Doppler-shifted energy spectrum in the Doppler-broadened spectra, p_z is the longitudinal momentum component of the annihilating electron-positron pair. A typcical line shape parameter for Doppler profile in aluminium is shown in Fig. 2.7.

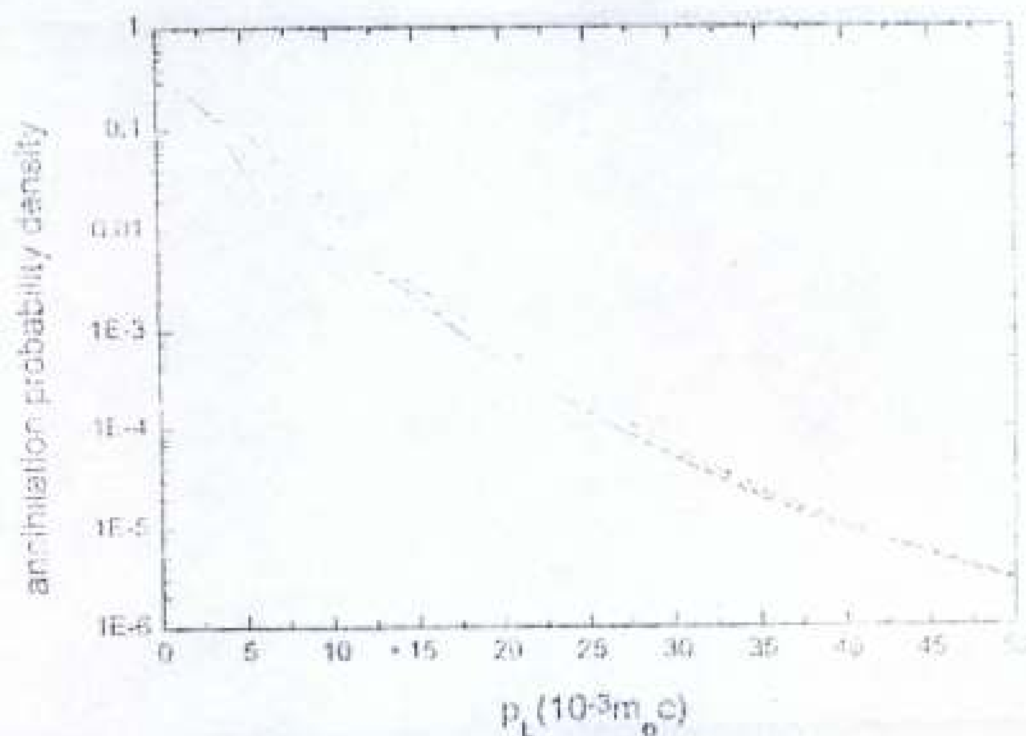

Fig. 2.7: Calculated values for the Doppler profile in aluminum. The solid line does not have any added detector broadening (Ghosh et al., 1999).

The quantitative evaluation can be carried out with specific lineshape parameters called S and W parameters. The determined lineshape parameters are defect specific, since they are determined by the local electronic environment of defects (Eichler and Krause-Rehberg, 1999).

2.11.1 S parameter

The S parameter is defined as the area of the central low-momentum part of the spectrum A_s, divided by the area below the whole curve after subtraction or cancellation of background effects due to source activity

$$S = \frac{A_s}{A_0} = \int_{E_0 - E_s}^{E_0 + E_s} N_D dE \Big/ \int^{peak} N_D dE \tag{2.34}$$

It gives the area under the central part of the profile, divided by the total area under the profile, as shown in Fig. 2.8. Thus a high value of S signals the presence of open-volume defects, whereas a low S value signifies a defect-free sample (Coleman, 2000).

It can be taken as the ratio between the number of counts in the center (511 ± 0.8keV) to the total peak area of the annihilation peak, where every kind of positron annihilation site yields a characteristic S parameter. That is to say, it is a measure of the momentum density at low momentum, since it is calculated as the ratio of low momentum region to the total region, in the obtained Doppler spectrum (Borner et al., 1999; Gebauer et al., 1999).

It is defined to parameterize the Doppler broadening of the positron annihilation line as

$$S = \left[\int_{511keV - I_s}^{511keV + I_s} f(\varepsilon) d\varepsilon \right] \Big/ \left[\int^{peak} f(\varepsilon) d\varepsilon \right] \tag{2.35}$$

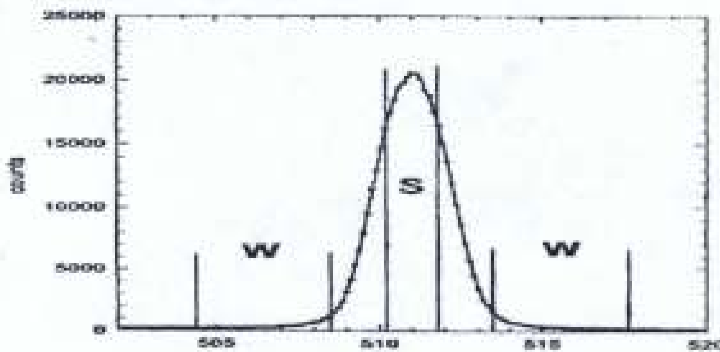

Fig.2.8: Doppler-broadening 511 keV peak measured for perfect silicon. The intervals used for defining S and W parameters are indicated (Coleman, 2000).

Hence it is the weighted sum of the bulk and defect S parameters, S_b and S_d respectively. The apparent S parameter is

$$S = (1 - \Omega) S_b + \Omega S_d \tag{2.36}$$

where Ω is the fraction of trapped positrons (positron annihilation fraction). It is the area under the spectrum in a narrow energy range symmetrical around 511keV. It mainly characterizes the positron annihilation with valence electrons.

The S parameter gives the area under the central part of the profile, divided by the total area under the profile. The W parameter gives the ratio between the area under each or both of the wings and the area under the profile. Hence, W parameter is used for profiling electrons with higher annihilation energy, i.e. high momentum or inner core electrons.

According to Saleh et al. (1999) values of the annihilation parameter S will be given by

$$\bar{S}(E)= F_s(E)S_s + \sum_{j=1}^{N} N_j(E)S_j + F_i(E)S_i + P_b(E)S_b \tag{2.37}$$

where S_j is the parameter for the jth layer given by

$$S_j = (S_F + K_j S_d)/(1+K_j) \tag{2.38}$$

S_F is the parameter for the defect free lattice, K_j is the trapping rate in the jth layer. S_d is the parameter for all defect contributions, $F_s(E)$ is the fraction of positrons reaching the surface, S_s, S_i and S_b are the parameters corresponding to 100% annihilation at the surface, interface and bulk respectively.

The measured S parameter is given by

$$S(E)=J_{ep}(E)S_{ep} + (1-J_{ep}(E))\bar{S}(E) \tag{2.39}$$

where

$$J_{ep}(E)= \int_0^{\infty} P(Z,E)e^{-z/L_{ep}}dZ \tag{2.40}$$

and L_{ep} is the epithermal positron scattering length, S_{ep} is the S parameter corresponding to epithermal positrons, J_{ep} is the epithermal positron scattering fraction.

The lineshape parameter S obtained from spectra acquired from variable implantation energy positron beam for a simple defect-free pure sample is given by

$$S(E) = J_s S_s + J_b S_b = J_s S_s + (1 - J_s) S_b \qquad (2.41)$$

and

$$J_S = \int_0^\infty P(Z,E) \exp\left(\frac{-Z}{L_+}\right) dZ \qquad (2.42)$$

$$J_b = 1 - J_s, \qquad (2.43)$$

$P(Z,E)$ is the positron implantation profile, S_s is the surface S parameter contribution to $S(E)$, J_s is the surface positron annihilation fraction, J_b is the bulk positron annihilation fraction, L_+ is the thermal positron scattering length.

The epithermal positron fraction reaching the surface is given by

$$J_{ep} = \int_0^\infty P(Z,E) \exp\left(\frac{-Z}{L_{ep}}\right) dZ \qquad (2.44)$$

where L_{ep} is the scattering length of an epithermal positron given by

$$L_{ep} = 3D_+ \Big/ \sqrt{\frac{3K_B T}{M^*}} \qquad (2.45)$$

T is temperature, M^* is positron effective mass. If S_{ep} is the characteristic lineshape parameter for positrons annihilating in the epithermal state, then (3.9) is rewritten by Saleh et al., (1999) as

$$S(E) = J_{ep} S_{ep} + (1 - J_{ep}) S_b = J_s S_s + (1 - J_s) S_b \qquad (2.46)$$

If there are various annihilation modes (in the defects, bulk and surface), the S parameter expressed as a combination of three terms is given as

$$S(E) = S_s F_s(E) + S_b F_b(E) + S_d F_d(E) \qquad (2.47)$$

where $F_s(E)$, $F_b(E)$ and $F_d(E)$ are the positron annihilation probabilities at the surface, bulk and defect respectively. S_s, S_b and S_d are the S parameters for surface, bulk and defect respectively.

The $f(E,x)$ F_s, F_b and F_d are related to the stationary density $n(x,E)$ of thermal positrons at incident positron energy E and at depth x, by the equations

$$\left.\begin{array}{l} F_s(E)=\lambda\int_0^\infty n(x,E)dx, \\ F_b(E)=D_+\left[\dfrac{dy(x,E)}{dx}\right]x, \\ F_d(E)=\sigma\int_0^\infty C(x)n(x,E)dx \end{array}\right\} \quad (2.48)$$

where λ is the bulk annihilation rate, D_+ is the diffusion constant, and σ, $C(x)$ are the specific trapping rate and defect concentration respectively,

$$C(x)=\frac{1}{\sqrt{2\pi}}\frac{1}{\sigma}\exp\left[\frac{-(x-\bar{d})^2}{2\sigma^2}\right] \quad (2.49)$$

$\bar{d}$ is the mean depth of positron implantation, and x is the width of sample cross-section. The Doppler parameter S as a function of positron implantation energy is shown for gallium arsenide in Fig. 2.9.

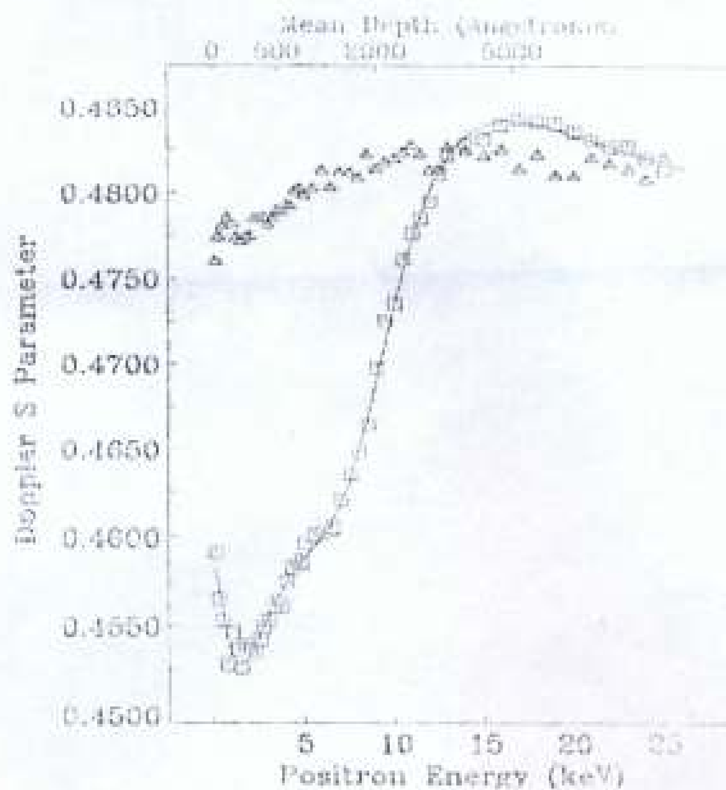

Fig.2.9: The Doppler parameter S plotted as a function of positron implantation energy for GaAs substrate (Rice-Evans et al., 1999).

For each annihilation mode with a characteristic probability F_i, and having a lineshape S_i, the observed S parameter is

$$S = \frac{\sum S_i F_i}{\sum F_i} \tag{2.50}$$

The superposition property of S allows us to write

$$S = \frac{S_s F_s + S_M (1 - F_s)}{\Omega} \tag{2.51}$$

where S_s is the S parameter corresponding to surface positron annihilation,

S_M is the S parameter for bulk positron annihilation, F_s is the probability for positron surface annihilation, and Ω is a normalization factor.

If F_{bulk} and F_f are the bulk and free positron annihilation probabilities, then

$$S_M = S_t F_t + S_{bulk} F_{bulk} \quad (2.52)$$

Also, S_s can be stated as

$$S_s = \frac{1}{4} F_0 Sp_s + (1 - F_0) S_{ss} \quad (2.53)$$

where S_t and S_{bulk} correspond to free and bulk lineshape parameters respectively, F_0 is the probability of surface positronium formation, S_{ss} is the S parameter associated with positron and valence electron surface annihilation, and Sp_s is the S parameter associated with positronium formation, and the normalization Ω is given by Gramsch et al., (1999) as

$$\Omega = (1 - F_s) + F_s\left(1 - \frac{3}{4} F_o\right) \quad (2.54)$$

In a near-surface defect region, the observed S parameter is given by

$$S(E) = J_s S_s + (J_d + J_i - J_s) S_i + (1 - J_d - J_i) S_b \quad (2.55)$$

and

$$S_i = \frac{S_b + K' S_d}{1 + K} \quad (2.56)$$

where J_s, J_d, J_i are the positron annihilation fractions in the surface, defect-region and interface respectively, S_s, S_b, S_d are the S parameters in the surface, bulk and defect-state respectively, S_i is the S parameter value associated with annihilation in the interface region, and K' and K are the trapping rates in the surface and bulk respectively (Saleh et al., 1999).

For a multilayer structure model, the value of the annihilation parameter is given as

$$\overline{S}(E) = F_s(E) S_s + \sum_{j=1}^{N} N_j(E) S_j + F_i(E) S_i + P_b(E) S_b \quad (2.57)$$

where S_j is the parameter for the jth layer given by

$$S_j = (S_{b'} + K_j S_d)/(1 + K_j) \quad (2.58)$$

where S_F is the parameter for the defect-free lattice, K_j is the trapping rate in the jth layer, S_d is the parameter for all defect contributions, $F_s(E)$ is the fraction of positrons reaching the surface, S_s, S_i and S_b are the parameters corresponding to 100% annihilation at the surface, interface and bulk respectively.

The measured S parameter is given by

$$S(E)=J_{ep}(E)S_{ep}+(1-J_{ep}(E))S(E) \tag{2.59}$$

where

$$J_{ep}(E)=\int_0^\infty P(Z,E)e^{-Z/L_{ep}}dZ \tag{2.60}$$

and S_{ep} is the S parameter corresponding to epithermal positrons, while L_{ep} is the positron scattering length given as

$$L_{ep}=3D_+ \Big/ \sqrt{\frac{3K_BT}{M*}} \tag{2.61}$$

where M^* is mass of positron, K_B is Boltzmann's constant and T is temperature.

The measured lineshape parameter may also be written as

$$S(E)=J_sS_s+J_fS_f+J_bS_b \tag{2.62}$$

where S_s, S_f and S_b are the characteristic S parameters corresponding to annihilation in the surface, film and bulk respectively.

For a uniform rectangular defect profile, the S parameter at a given energy can be expressed as

$$S(E)=J_sS_s+\sum_{i=1}^{n}J_iS_i+J_bS_b \tag{2.63}$$

where S_i is the S parameter corresponding to the jth layer, and is given by

$$S_i = \left(\frac{S_b + K_i S_d}{1 + K_i}\right) \tag{2.64}$$

with J_s, J_i and J_b the trapping fractions at the surface, interface and bulk respectively, S_s and S_d are the S parameters corresponding to the surface and defect states respectively, and K_i is the trapping rate at the interface. The S parameter of a composite material is given by

$$S_{comp} = F_{cluster}(E)S_{cluster} + F_{host}(E)S_{host} \tag{2.65}$$

where $S_{cluster}$ and S_{host} are the bulk S parameters of the nanocluster and the embedding material respectively, making up the composite material, and $F_{cluster}$, F_{host} are the annihilation fractions in the nanocluster and embedding host respectively, with

$$F_{cluster}(E) + F_{host}(E) = 1 \tag{2.66}$$

The assumption is that the composite material is defect free, and positrons do not annihilate at the cluster-host interface (van Huis et al., 2002).

2.11.2 W parameter

The W parameter is the area of the Doppler curve in a fixed energy interval A_w divided by the area below the whole curve A_0, taken in a high momentum region far from the centre, and is given as

$$W = \int_{E_1}^{E_2} N_D dE \Big/ \int^{peak} N_D dE \tag{2.67}$$

It is the sum of the areas under the wings of the spectrum, i.e. in two regions symmetrical around 511keV, as shown in Fig. 2.10. It mainly characterizes the positron annihilation with core electrons. It is equally taken as the ratio between the wing areas ($2.76keV < |E_\gamma - 511keV| < 3.96keV$) to the total peak area, or the ratio of high momentum region ($15 \times 10^{-3} m_0c < |p_L| < 20 \times 10^{-3} m_0c$) to the total Doppler region, as it is a measure of the momentum density.

It can also be defined as

$$W=\left[\int_{511keV-I_w-\Delta I_w}^{511keV-I_w} F(\varepsilon)d\varepsilon+\int_{511keV+I_w}^{511keV+I_w-\Delta I_w} F(\varepsilon)d\varepsilon\right]\Big/\left[\int^{peak} F(\varepsilon)d\varepsilon\right] \tag{2.68}$$

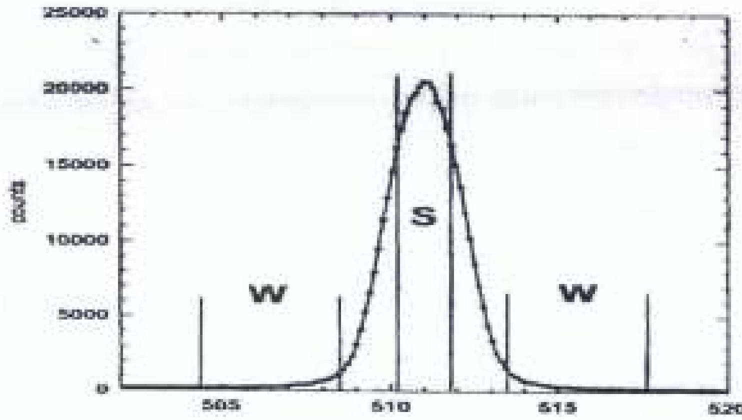

Fig. 2.10: Doppler-broadening 511 keV peak measured for perfect silicon. The intervals used for defining S and W parameters are indicated (Coleman,2000).

Hence it is the composite sum of the W parameters corresponding to bulk and defect states, and also given as

$$W=(1-\Omega)W_b+\Omega W_d \tag{2.69}$$

where W_b and W_d are the W parameters corresponding to the bulk and defect states respectively (Krause-Rehberg and Leipner, 1999; Eichler and Krause-Rehberg, 1999).

The magnitude of core electron-positron annihilations can be investigated using the parameterization

$$W=A_w\Big/A_{tot}=\int_{\theta_1}^{\theta_2} F(\theta_Z)d\theta_Z\Big/\int_0^{\infty} F(\theta_Z)d\theta_Z \tag{2.70}$$

where the A_w, A_{tot} are areas under the measured Doppler curve. The boundaries θ_1 and θ_2 are chosen in such a way that W reflects mainly core electron annihilations, and assume θ_1 = 15mrad (ΔE=3.8keV) and θ_2 = 20mrad (ΔE=511keV). When differences in the shape of the

curve are negligible, large changes may still be observed in the W parameter (Alatalo et al., 1995). A typical plot of W parameter with incident positron energy is shown in Fig. 2.11.

The theoretical equivalent of the experimentally obtained W parameter as stated above, is

$$W = \sum_i \lambda_i \left(\frac{A_w}{A_{tot}} \right)_i \bigg/ \lambda_{tot} \qquad (2.71)$$

where λ_i *and* λ_{tot} are the core-state and total annihilation rates respectively, in the observation window $\theta_1 < \theta < \theta_2$ (Alatalo et al., 1995).

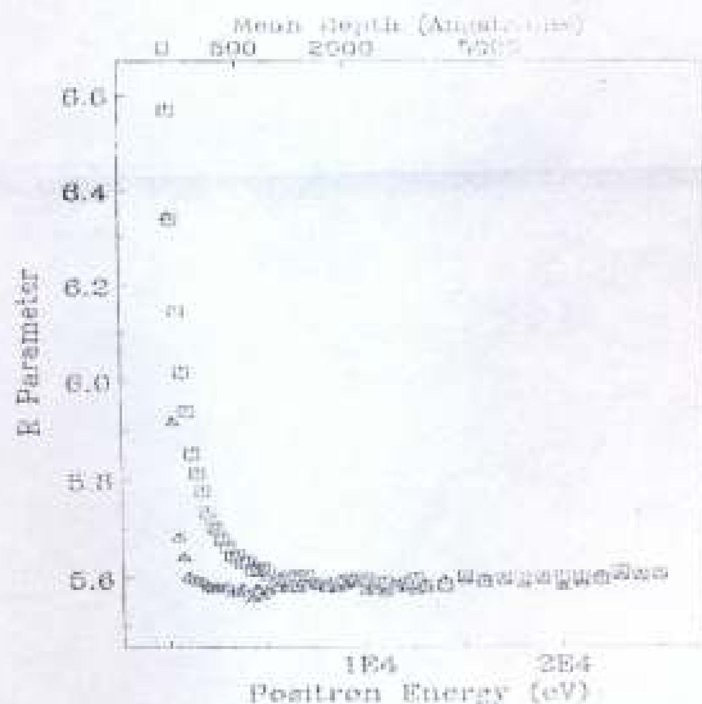

Fig. 2.11: Doppler parameter W plotted as a function of positron implantation energy for GaAs substrate (Rice-Evans et al.,1999).

Usually, the lineshape parameters are normalized with the typical parameters for defect-free materials. The advantage of this normalization is that, independent of the chosen limits for the determination of S and W from the Doppler spectrum, the obtained values can be compared. This, however, does not hold for the comparison of values measured with different spectrometers. The reason is the dependence of the normalized lineshapes on the resolution of

the spectrometer. The W parameter is more sensitive to the chemical surroundings of the annihilation site than the S parameter, because the core electrons having a high momentum are contributing mainly in the region of large energy deviations from the annihilation energy of E_γ. Both parameters are sensitive to the concentration and kind of defects. The normalized S parameter characterizing the Si divacancy varies between 0.33 and 0.5 if the Full Width at Half Maximum (FWHM) varies between 1.5 and 1.1keV respectively. The normalized W parameter for the Si divacancy is calculated to be 0.076 and 0.084 for a Full Width at Half Maximum (FWHM) of 1.5 and 1.1keV (Eichler and Krause-Rehberg, 1999).

2.11.3 S/W parameter

In order to obtain the defect concentration, one has to presume the defect type, i.e. from S_d and W_d parameters. A new parameter R, which depends only on the defect type, can be used to obtain the defect concentration, and is defined by Krause-Rehberg and Leipner, (1999) as

$$R = \left|\frac{S - S_b}{W - W_b}\right| = \left|\frac{S_d - S_b}{W_d - W_b}\right| \qquad (2.72)$$

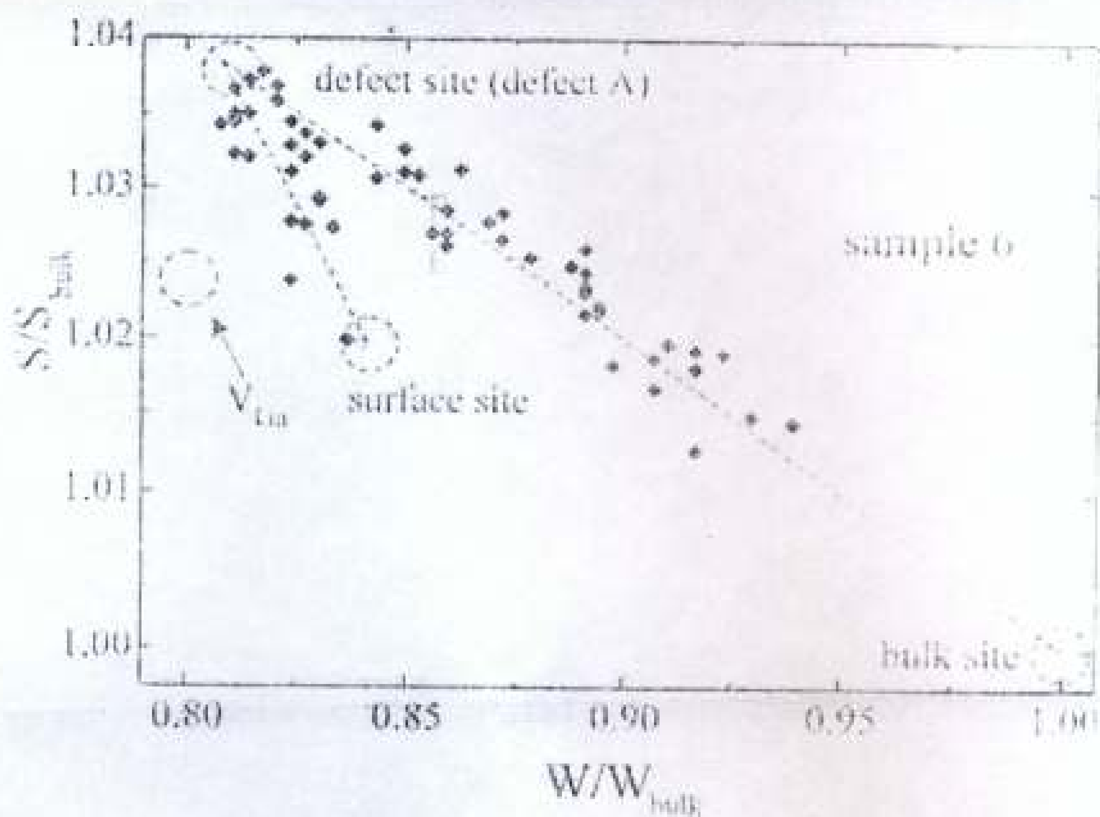

Fig. 2.12: S versus W plot of positron energy scan (0-40 keV) for GaAs (Borner et al., 1999).

(S, W) plots are used to identify open-volume defects. A straight line is obtained in the (S,W) plot between the characteristic points of the surface and the defect. A second straight line is obtained between the defect and bulk states. With increasing incident energy, i.e. increasing depth, the (S,W) curve runs clockwise through different states. All positrons implanted into a medium are trapped in implantation defects. An S versus W plot for GaAs is shown in Figs. 2.12 and 2.13.

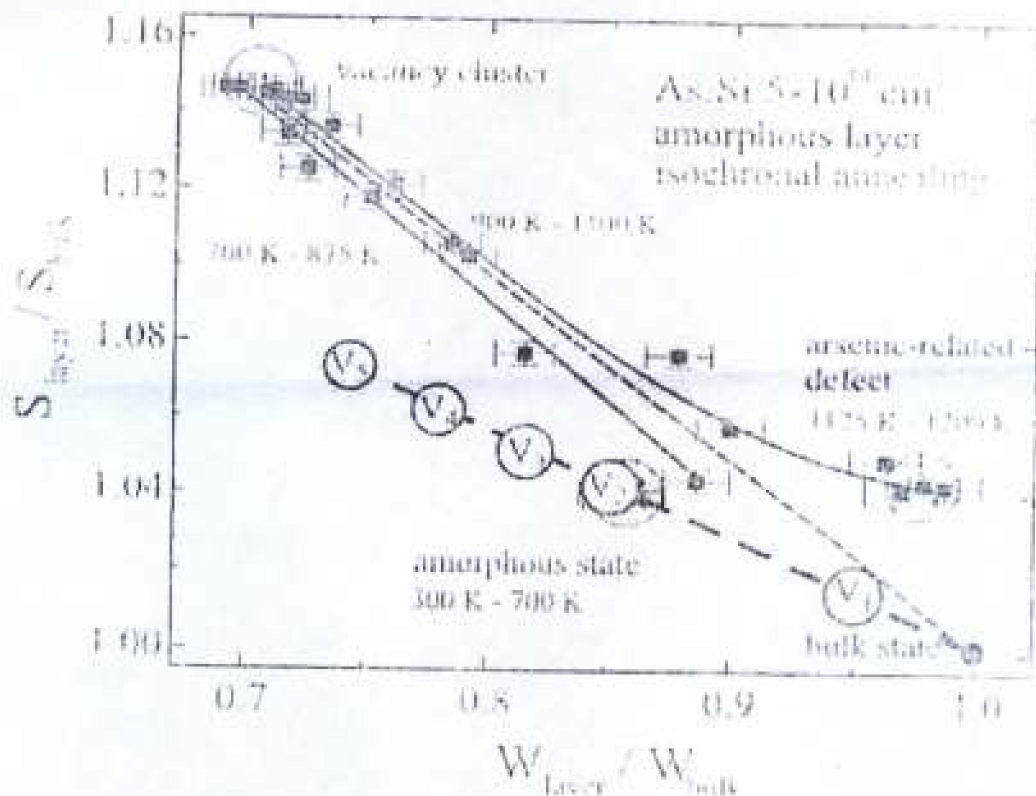

Fig 2.13: S versus W plot of the annealing behaviour of as-grown silicon (Eichler and Krause-Rehberg, 1999).

The bulk R parameter is observed for the highest positron energies, because almost all positrons reach the defect-free region beneath the damaged layer (Borner et al., 1999).

2.12 Factors Affecting Lineshape Parameters

2.12.1 Temperature

For a plot of S and mean lifetime τ as a function of temperature, the S parameter increases steadily from between 0.425 to 0.440 up to a temperature of 1270K. The mean lifetime decreases steadily from between 115 to 135ps up to the same temperature 1270K. That is, most positron annihilation in the free state and hence, positron lifetime, strongly depend on trapping by vacancy-type defects. The decrease in the lifetime of positrons trapped by vacancy-type defects suggests an increase in the density of electrons in such defects. The change in the

electronic density could be due to changes in the electronic configuration of atoms near the defect.

For Si, the normalized lineshape parameters S_s/S_b and W_s/W_b change only weakly or steadily up to 700K. They are close to the theoretically obtained parameters for the Si divacancy. Above 875K, the S parameter increases continuously to a level of 0.45, which corresponds to a large open-volume of the positron trapping centre. Between 1125K to 1270K, the S parameter keeps constant, or changes rather very weakly (Jain et al., 1999 and Gramsch et al., 1999).

The comparison with the theory data shows that open-volume defects are only detectable up to 750K. Likely, the positron trapping is saturated in defects in this case. At higher temperatures, further defect reactions occur. The W parameter abruptly decreases at 875K. Hence, the exact identification of isolated vacancy-like defects in Si is not possible for an unknown trapping rate or energy resolution. The comparison between experimentally obtained and theoretically determined lineshape parameters for isolated defects shows a good agreement (Brusa et al., 2000 and Uedono et al., 1999).

2.12.2 Implantation energy

At high energies above 15keV, S approaches a constant value, indicating that almost all positrons are implanted into the bulk in this energy range and annihilate without diffusing back to the surface. The value of S increases with decreasing energy, showing positronium and positron annihilation at the surface. The value of S near the surface increases with increasing temperature, due to the increase in the formation probability of positronium due to the thermal desorption of positrons from the surface state.

The characteristic diffusion length is found to be $1440A^0$. The gradient of the measured S value slopes in the region 1-3keV reflect the changes in the diffusion length as a consequence of the concentration of vacancies present. The increases in the S values at 3-5keV indicate the

trapping of positrons within the implanted region, signaling the presence of open-volume defects. The defect-free bulk S parameter is reached way beyond 15keV. Above 20keV, all the samples tend toward the same S parameter characteristic of defect-free Si bulk material, indicating that the majority of positrons are implanted deeply enough such that they annihilate beyond the ion-induced defect layer.

The W parameter increases steadily to a value at a positron energy of 22keV within a depth of 0-5000A^0, for GaN and GaAs. The high value of S beyond 20keV corresponds essentially with annihilation at the substrate. The sharp rises to the broad maxima in W at about 15keV indicate significant trapping at interface defects (Rice-Evans et al., 1999; Uedono et al., 2000).

2.12.3 Energy resolution

The choice of the interval limits of the lineshape parameter determination is important for the sensitivity of the measurements. The influence of the interval limits on the S parameter is stronger for high energy resolution. That is, for a high S parameter sensitivity measurement, the interval limit is small for high energy resolutions. This is valid too for the dependence of the normalized W parameter on the interval limit (Eichler and Krause-Rehberg, 1999).

2.12.4 Mean depth

For a plot of S with mean penetration depth D, there is a decrease of S with increasing depth, on spikes, obtained experimentally for GaAs. This clearly portrays a disordered growth structure in the underlying layers of GaAs, i.e the positron annihilation rate at the surface is very high, and there is high positron annihilation rate at open-volume defects in the depth.

A detected larger S parameter relative to W in the(W,S) plot of GaAs indicates the observation of a certain defect type which could be small a vacancy cluster (Gebauer et al., 1999; Borner et al., 1999).

CHAPTER THREE

METHODOLOGY

In this chapter, a description of how the research work was carried out is explained.

3.1 Modeling of S Parameter

From the study of the experimental data and available literature, the factors that the positron annihilation characteristics (S parameter, W parameter and penetration depth) depend on were obtained. Studies revealed that the annihilation parameters depend on:

i) density of the material

ii) thickness of the material

iii) illumination time (for materials that are illuminated or exposed to different forms of radiation).

The penetration depth of the material was found to depend on the density of the material, and on the energy of the incident positrons. Models were developed to predict or model the S and W parameters of different materials.

From the study, the dependence of the S parameter on the density of the material was obtained as

$$S(\rho) = [(0.84(14.5\ln\rho - 2.2)\exp(-\rho)) - 0.385]^{\frac{1}{5}} \tag{3.1}$$

where ρ is the density of the material.

The dependence of the S parameter on the thickness of the material was obtained as

$$S(T) = \frac{\left(4 - \frac{\log T}{10}\right)\log T}{2\ln T} \tag{3.2}$$

where T is the thickness of the material.

For materials that are illuminated, the S parameter dependence on the illumination time was obtained as

$$S(I) = \left[9.8\sin \log(90 + I)) \frac{\pi}{180} \right]^{\frac{1}{5}} \tag{3.3}$$

where I is the illumination time for the material.

The S parameter dependence on the penetration depth and on the incident positron energy was obtained as

$$S(D) = S(E) = \left[\left(2.33 + \frac{\log 60X}{600} \right) \times \log A \times \exp(-\log A) \right]^2 \tag{3.4}$$

where D and E are the penetration depth and incident energy respectively, and

$$\left.\begin{array}{l} A = \dfrac{35X}{3.4}, \\ X = \dfrac{16 + \log D}{19}, \\ D = \dfrac{40E^{1.6}}{\rho} \end{array}\right\} \tag{3.5}$$

ρ is the density of the sample material.

3.2 Modeling of W Parameter

Also from the study, the dependence of the W parameter on the density of the material was obtained as

$$W(\rho) = [7.61\rho\exp(-\rho)]^{-1} \tag{3.6}$$

where ρ is the density of the material.

The dependence of the W parameter on the thickness of the material was obtained as

$$W(T) = 0.2\log T(4.51 - \log T) \tag{3.7}$$

For materials that are illuminated, the W parameter dependence on the illumination time was obtained as

$$W(I) = \left[0.72112 + \frac{\log(1.01+I)}{18.7}(\cos\log(1.01+I))\right]\frac{\pi}{180} \tag{3.8}$$

where I is the illumination time.

The W parameter dependence on the penetration depth and incident positron energy was obtained as

$$W(D) = W(E) = 0.43\left[-(2+\frac{\log 60B}{600})\times(-\log A)\times\exp(-\log A)\right]^{-2} \tag{3.9}$$

where D and E are the penetration depth and incident energy respectively, and

$$\left.\begin{aligned} A &= \frac{60B}{3.4}, \\ B &= \frac{\log(1+E)^{0.35}}{2.05}, \\ D &= \frac{40E^{1.6}}{\rho} \end{aligned}\right\} \tag{3.10}$$

and ρ is the density of the sample material.

A FORTRAN computer programme was developed to test the various expressions put forward for the dependence of the S and W parameters on the density of the material, thickness of the material, illumination time, incident positron energy and positron penetration depth.

CHAPTER FOUR

RESULTS AND DISCUSSION

4.0 Introduction

The models proposed in Chapter Three were tested for metals and elemental semiconductors. Results of experimental research work at the Slow-positron Beam Laboratory at the Department of Physics, University of Cape Town, South Africa, was used to test the models. Aluminum was the choice metal, based on its varied industrial and technological applications. Amorphous silicon was the elemental semiconductor of choice, as informed by its extensive application in the electronics industry and information systems.

For each of aluminum and amorphous silicon, the S and W parameters obtained as a result of their respective mathematical models, were compared with results obtained from the experimental research work on Doppler-broadened slow positron beam, as already mentioned above. Both S and W parameters depend on the illumination time I, material density p, positron implantation energy E, positron penetration depth D and sample thickness T.

Figure 4.1 shows the variation of modeled and experimental S parameters with penetration depth for silicon. As revealed in the figure, the experimental S parameter is more scattered. This is due to experimental errors. The modeled S parameter for silicon follows a definite trend. When the penetration depth is less than 100nm, there is a poor agreement between the modeled and experimental S parameters. This is the surface and near-surface region. When the penetration depth is greater than 200nm, there is a good agreement between the modeled and experimental S parameters. This is the bulk, interface and substrate regions. Statistically, a correlation of 0.72 was obtained between the modeled and experimental S parameters.

The variation of the modeled and experimental S parameters with penetration depth for aluminum is shown in Figure 4.2. As revealed by the figure, there is a good agreement between the modeled and experimental S parameters when the penetration depth is more than 200nm. But

for penetration depth less than 200nm, the modeled and experimental S parameters are not in good agreement. The correlation between the modeled and experimental S parameters is 0.92. Figures 4.1 and 4.2 reveal that the model could be useful in studying the variation of S parameter with penetration depth in the bulk, interface and substrate regions.

Figure 4.3 shows the variation of modeled and experimental S parameters with implantation energy for silicon. As seen in the figure, when the implantation energy is greater than 6keV, there exists a good agreement between the modeled and experimental S parameters. As the implantation energy is directly varying with the penetration depth, this corresponds to the bulk, interface and substrate regions. At less than 6keV, their agreement is relatively poor, as a low S parameter value of 0.410 could not be obtained with the model. The experimental value in the figure is quite scattered. This may be due to poor vacuum conditions. A correlation of 0.85 was obtained between the modeled and experimental values, showing that the model could predict well the variation of S parameter with implantation energy.

Figure 4.4 shows the variation of modeled and experimental S parameters with implantation energy for aluminum. As revealed by the figure, at less than 6keV, there is a fair agreement between the modeled and experimental S parameters. But when the implantation energy is more than 6keV, there is a nearly-perfect agreement between the modeled and experimental S parameters. A statistical correlation of 0.92 was obtained for this. Figures 4.3 and 4.4 therefore prove the models could be useful in studying the variation of S parameter with implantation energy for the bulk, interface and substrate regions. The model is in perfect agreement with experimental values in the bulk region.

Figure 4.5 reveals a one-to-one agreement between the variation of the modeled and experimental S parameters with illumination time for silicon sample. This shows that the model can be successfully used to predict or calculate the S parameter of amorphous semiconductors that are illuminated with electromagnetic radiation.

But in figure 4.6, there is a fairly good agreement between the modeled and experimental W parameters with penetration depth for silicon. As revealed in the figure, there is a good agreement between the modeled and experimental values in the surface and bulk regions. In the figure, the experimental W parameter is quite scattered, and does not follow a particular trend, unlike the modeled W parameter. This may be due to changes in voltage supply and in the atmospheric conditions in the laboratory. A correlation of 0.74 was obtained between the modeled and experimental W parameters.

Figure 4.7 shows the variation of the modeled and experimental W parameters with penetration depth for aluminum. As revealed in the figure, there is a very good agreement between the modeled and experimental W parameters, from the surface region, into the bulk region. A correlation of 0.89 was obtained between the modeled and experimental values, showing the model can predict well the variation of W parameter with penetration depth for metals, both at the surface and bulk regions.

In figure 4.8, the variation of modeled and experimental W parameters with implantation energy for silicon is shown. The figure reveals that there is a fairly good agreement between the modeled and experimental W parameters in the surface and bulk regions. The experimental W parameter did not follow a definite trend, unlike the modeled W parameter. In the interface and substrate regions, there is a poor agreement between the experimental and modeled W parameters for silicon. A correlation of 0.77 was obtained between the modeled and experimental W parameters for silicon.

The variation of the modeled and experimental W parameters with implantation energy for aluminum is shown in figure 4.9. In this figure, the modeled and experimental W parameters were in good agreement in the bulk, interface and substrate regions, with a correlation of 0.81 between the modeled and experimental W parameters. In the surface region, there is a poor

agreement, as the model could not reproduce the experimental W parameters in this energy range.

The variation of the modeled and experimental W parameters with illumination time for silicon is shown in figure 4.10. In the figure, there is a correlation of 0.99 between the modeled and experimental W parameters. The good agreement between the modeled and experimental W parameters with illumination time may be due to the fact that illuminating silicon with electromagnetic beam creates defects and structural ordering which is measured by the beam system.

4.1 Results of S Parameter

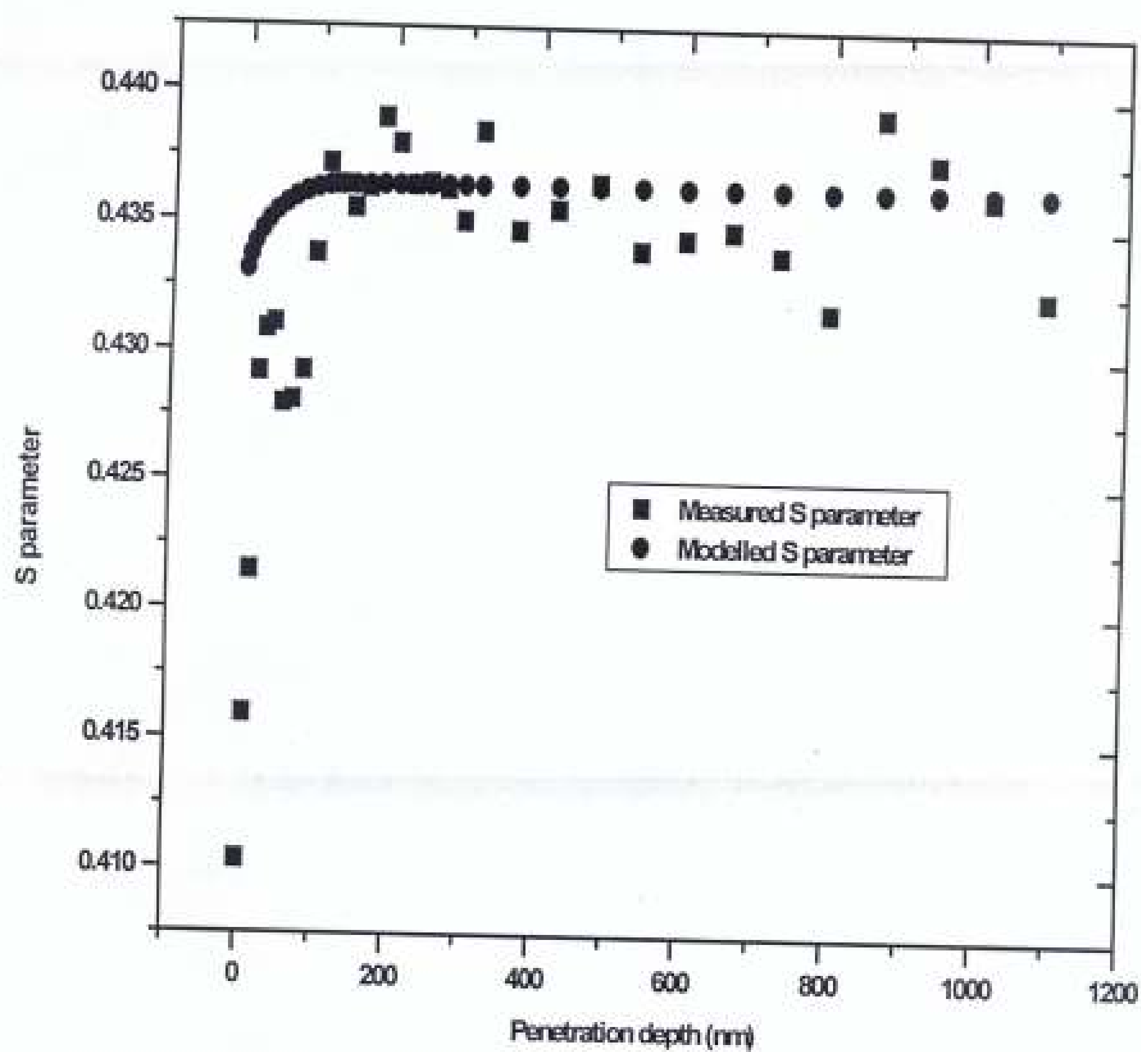

Fig. 4.1: Variation of S parameter with penetration depth for silicon

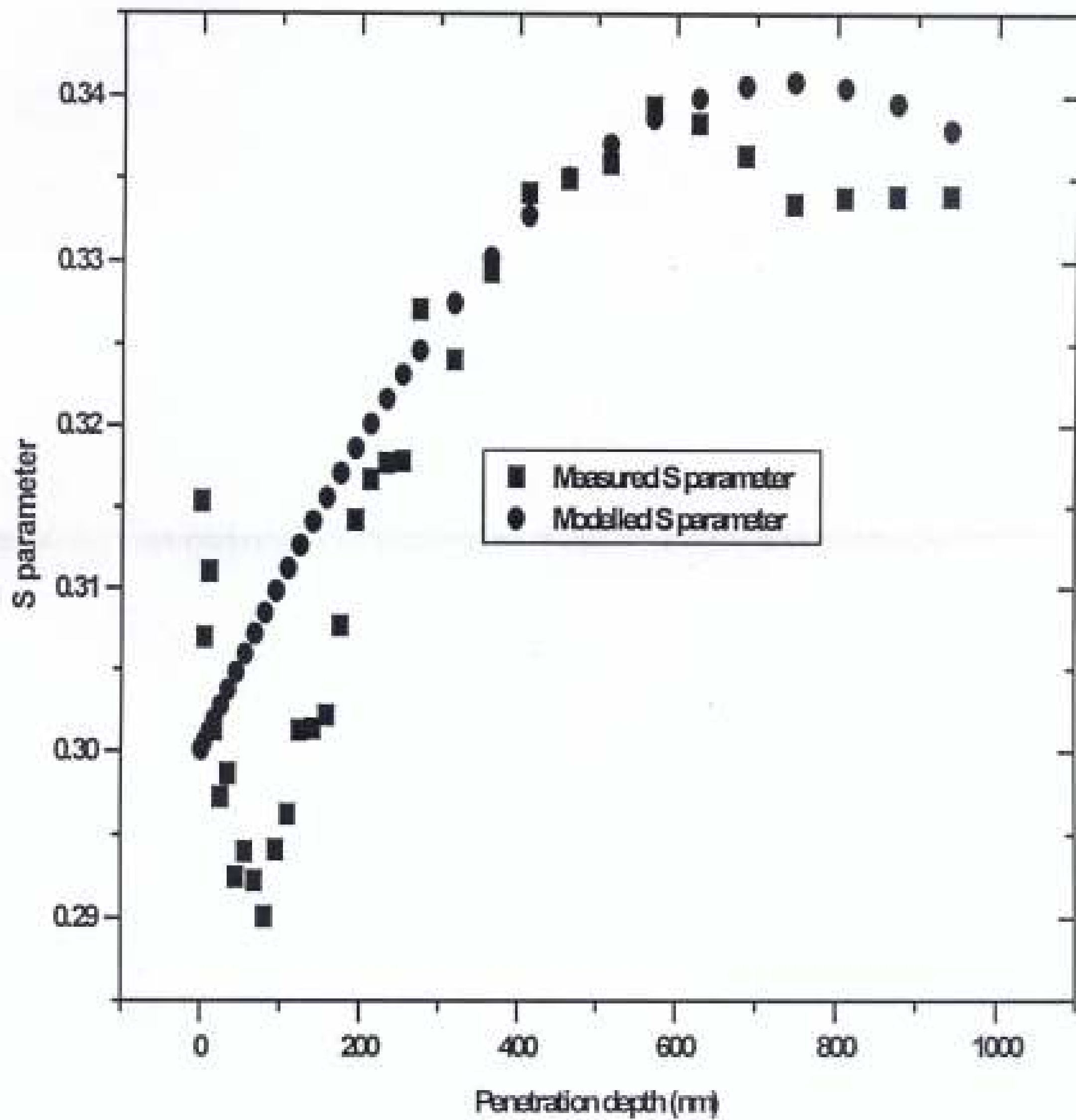

Fig. 4.2: Variation of S parameter with penetration depth for aluminium

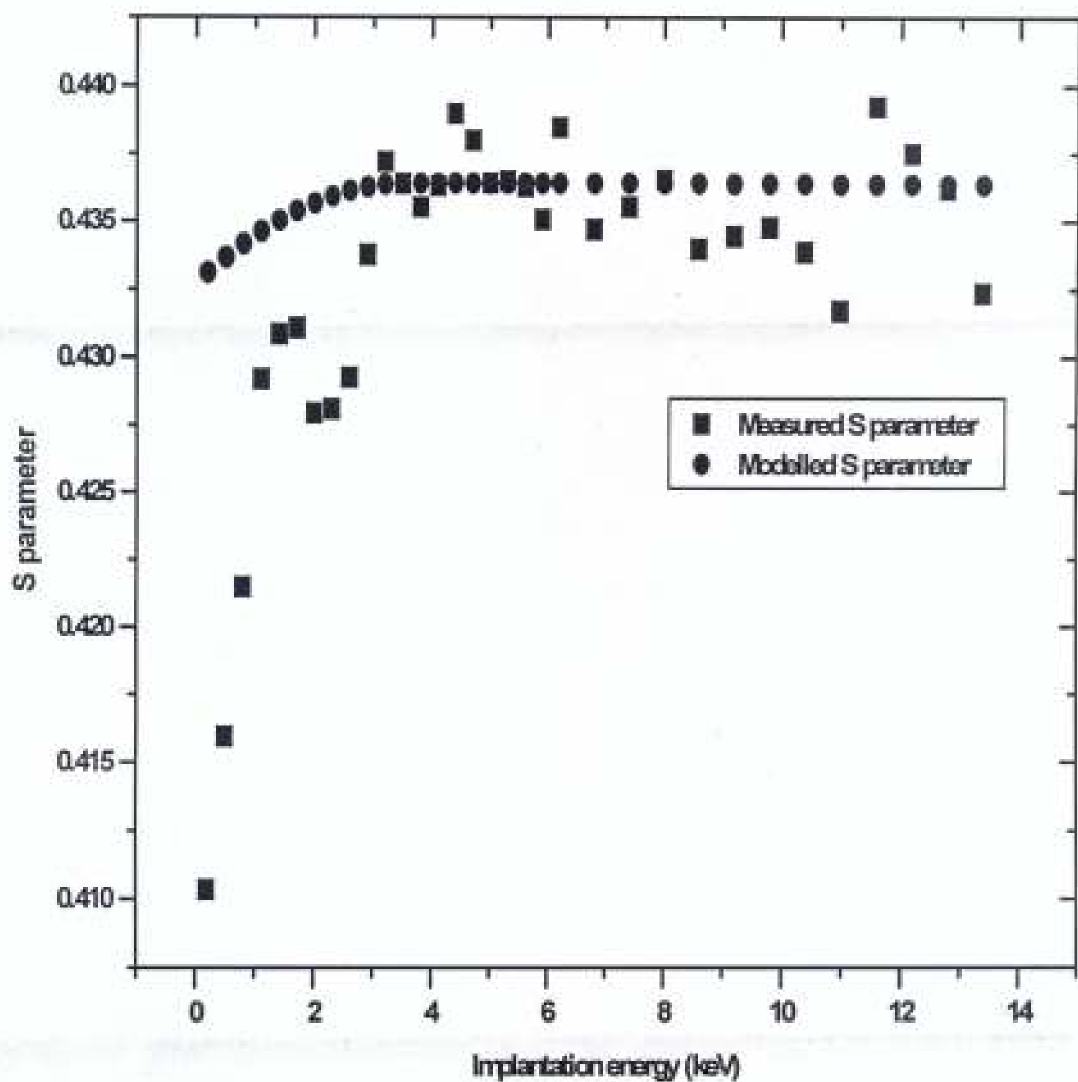

Fig. 4.3: Variation of S parameter with implantation energy for silicon

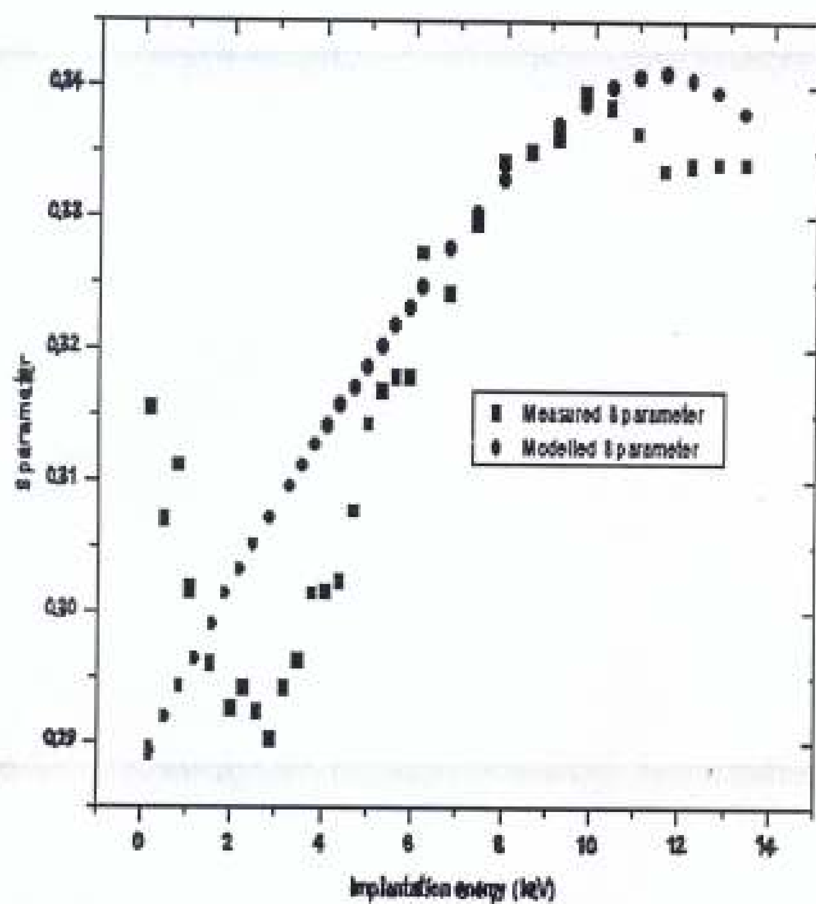

Fig. 4.4: Variation of S parameter with implantation energy for aluminium

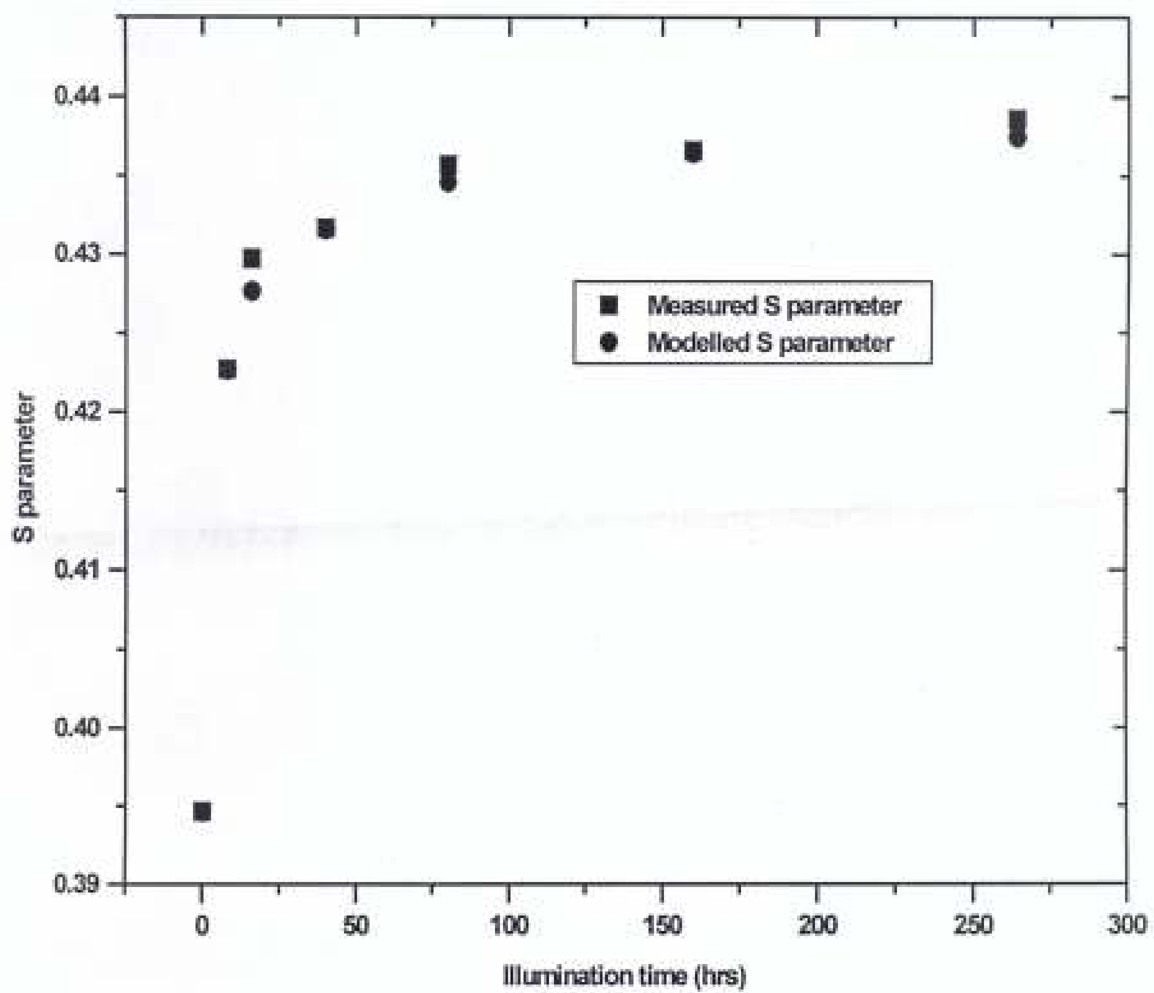

Fig. 4.5: Variation of S parameter with illumination time for silicon

4.2 Results of W Parameter

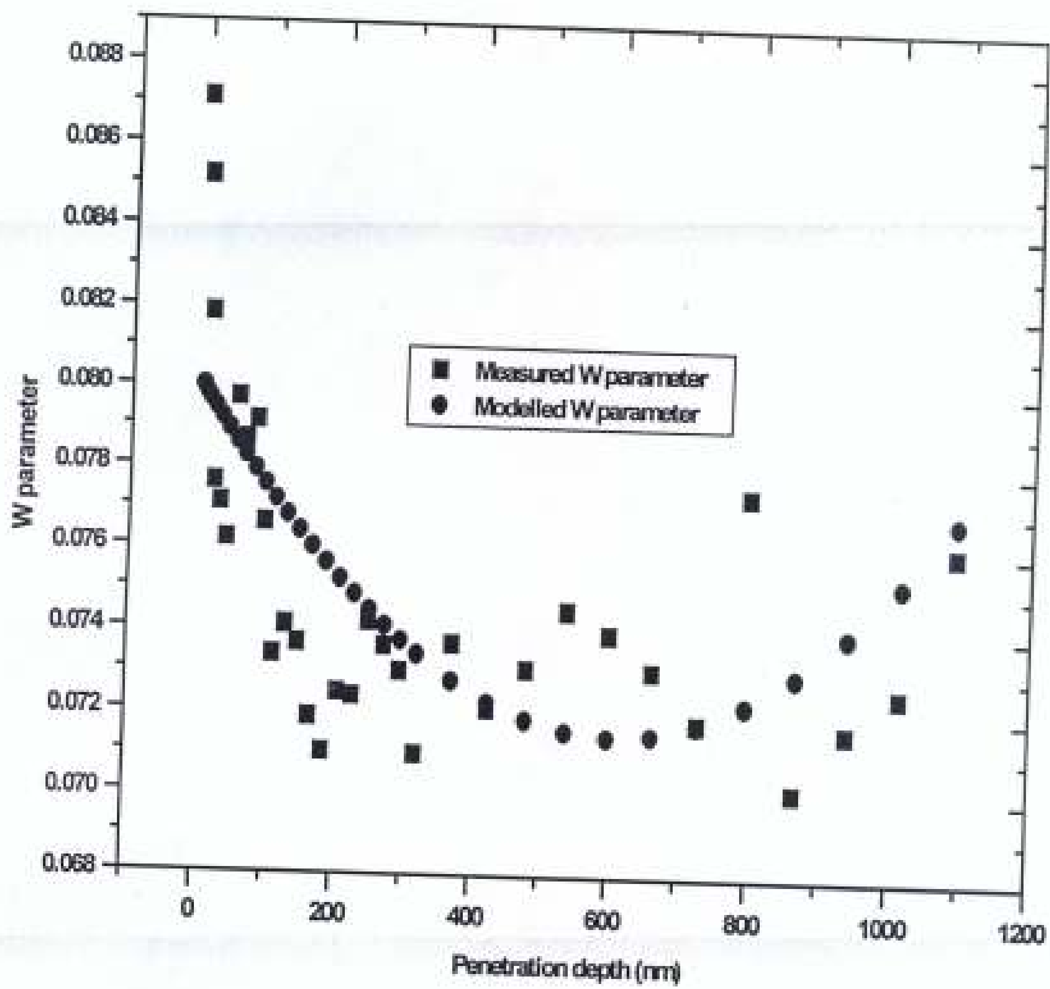

Fig. 4.6: Variation of W parameter with penetration depth for silicon

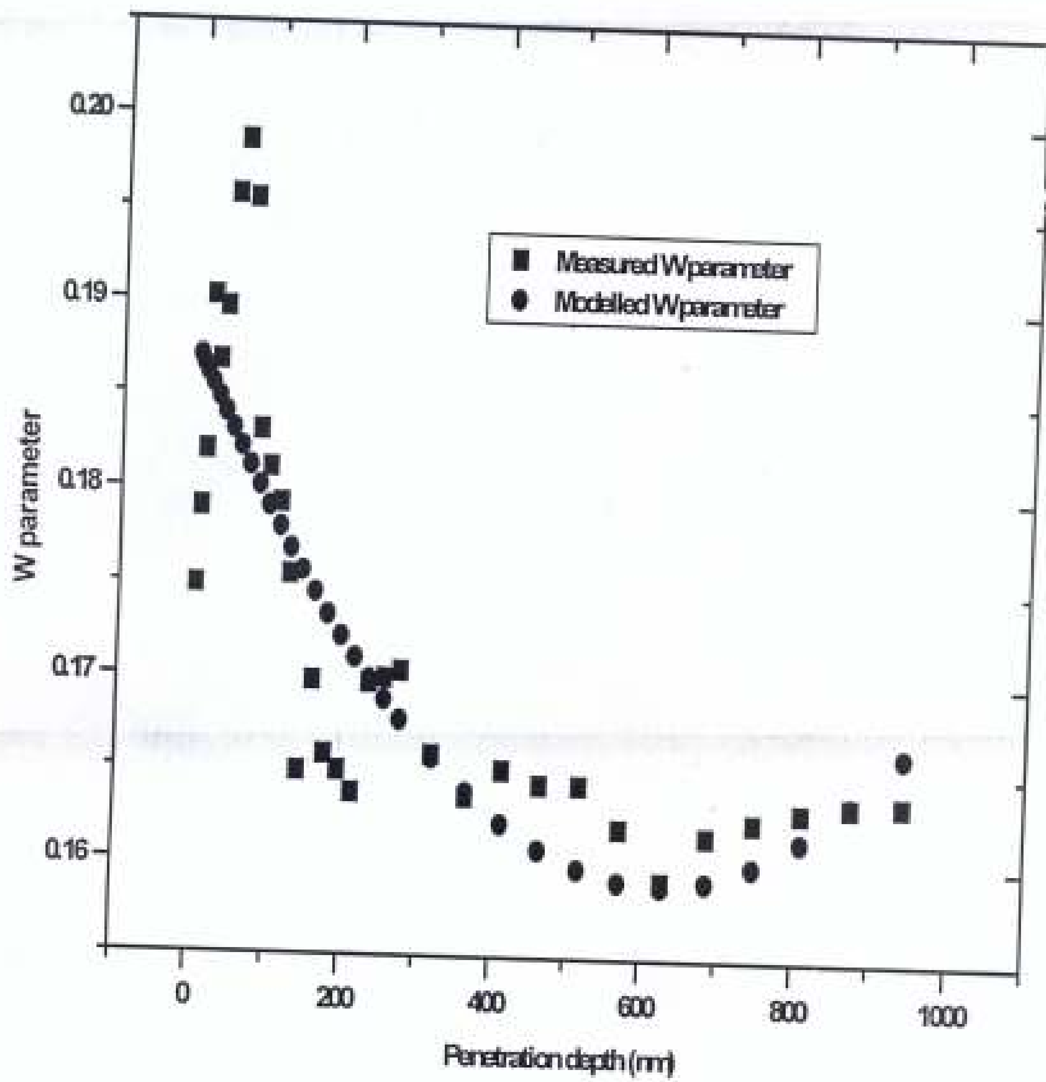

Fig. 4.7: Variation of W parameter with penetration depth for aluminium

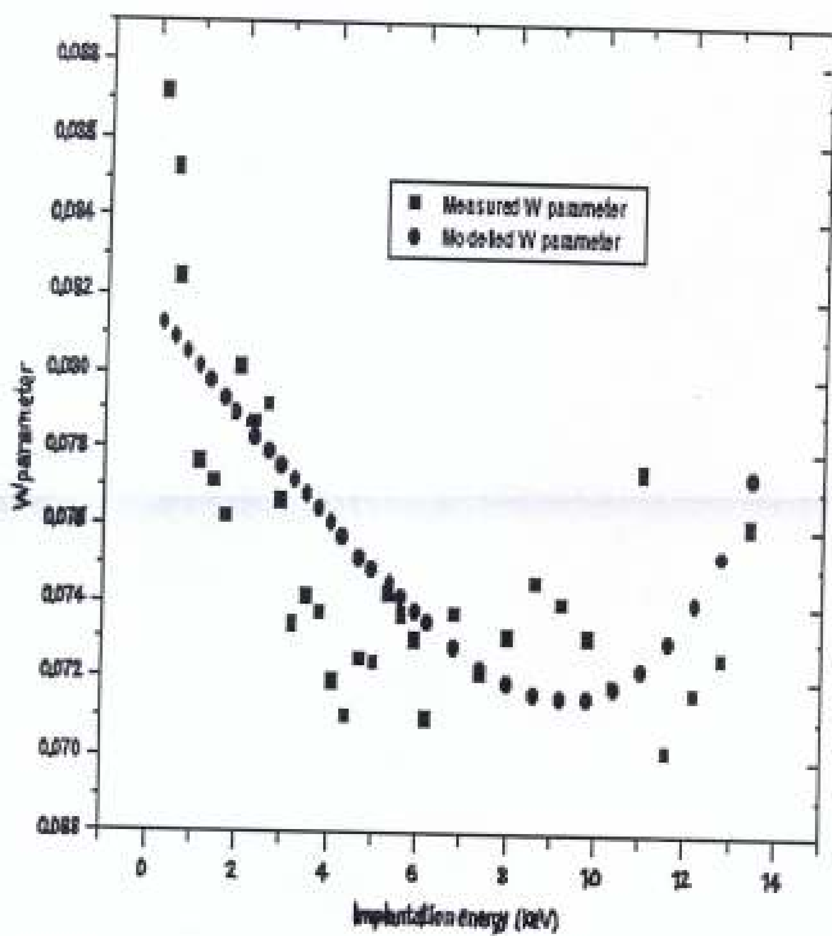

Fig.4.8: Variation of W parameter with implantation energy for silicon

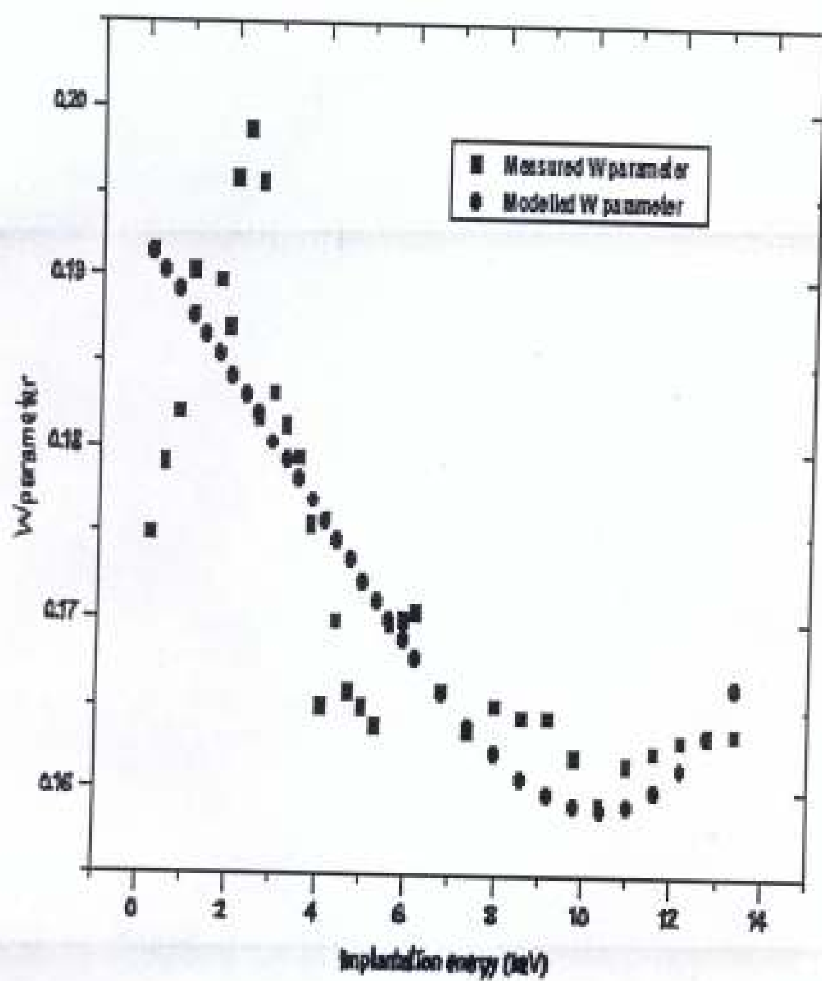

Fig.4.9: Variation of W parameter with implantation energy for aluminium

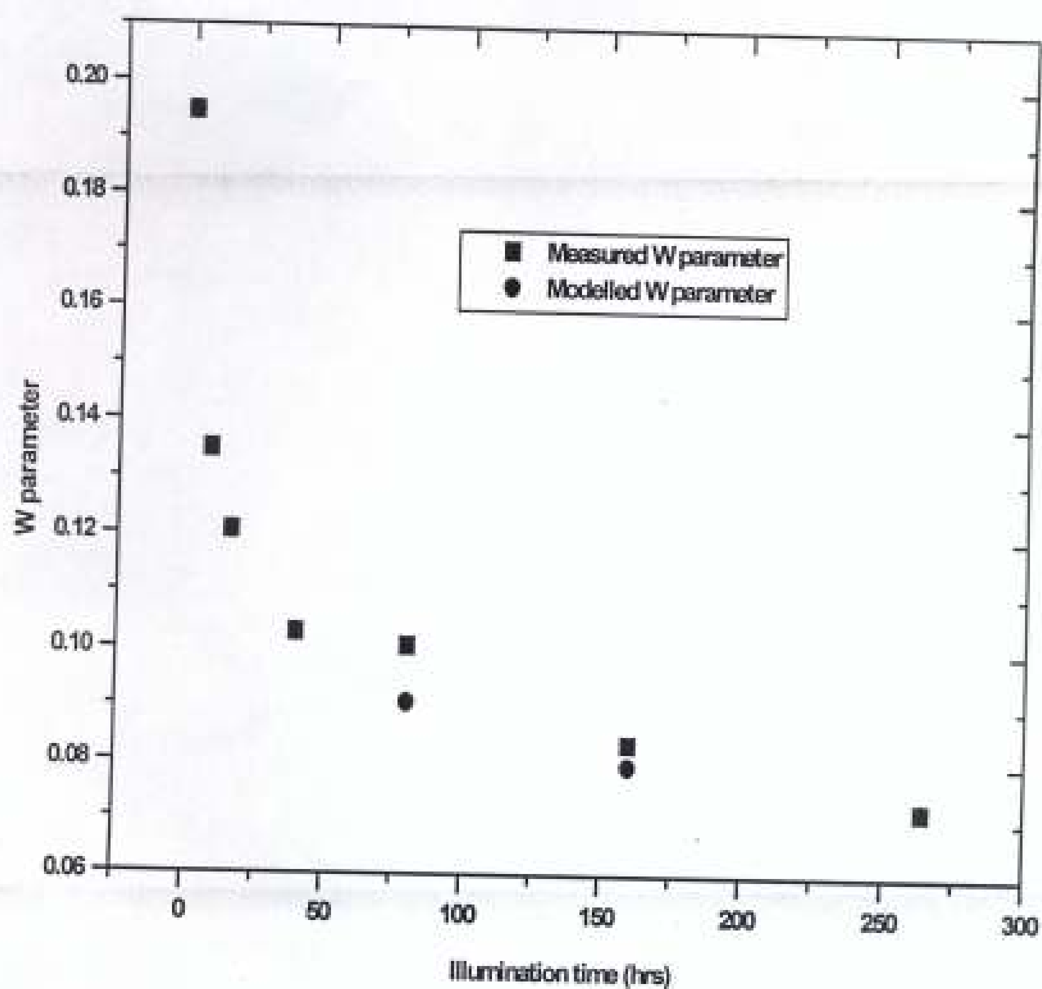

Fig. 4.10: Variation of W parameter with illumination time for silicon

CHAPTER FIVE

CONCLUSION

5.1 General Conclusion

In this work, models for the calculation of S and W parameters of metals and elemental semiconductors have been proposed. Also, the modeled S and W parameter variation with implantation energy or penetration depth was investigated with the corresponding experimental S and W parameter variation with implantation energy or penetration depth. The S and W parameters for metals and elemental semiconductors depend on the thickness of the sample material, density of the material, the illumination time of the sample, and the positron implantation energy (or positron penetration depth). From the study, it was found that incorporating components of the above mentioned characteristics into the models of S and W parameters helped to stabilise the high sensitivity of the S and W parameter variation with positron implantation energy or positron penetration depth. Good comparisons were obtained between the variation of modeled S and W parameters and the corresponding variation of experimental S and W parameters with positron implantation energy or positron penetration depth.

The modeled S parameter increase with positron implantation energy and penetration depth is of the form expx/x, up to a maximum of 0.437 across the surface, after which the modeled S parameter reduces gradually from the surface to the interface, and into the bulk of the sample material. The interface between the surface of the material and its bulk is generally acceptable as between 300nm to 600nm from the topmost layer of the sample's surface.

The model for W parameter proposes a decrease of the W parameter with implantation energy and penetration depth, down to a minimum of 0.301, through the surface, after which the W parameter increases gradually from the interface, through the bulk of the sample. From the

available plots, the interface can be deduced to be between 300nm to 600nm from the topmost layer of the sample's surface.

5.2 Applications of Results

The results obtained in this work will be useful in the study of defects, defect density and structural characterisation of metals and semiconductors. The proposed models can be used in conjunction with electron microscopy and x-ray diffraction for the defect structural characterisation of metals and semiconductors.

Furthermore, the results obtained in this work will be useful in the development of a comprehensive code for characterisation of materials.

5.3 Conclusion

Models were proposed for the calculation of S and W parameters of metals and semiconductors. The proposed models were successfully tested and found to be in good agreement with experimental values obtained at the Slow-positron Beam Laboratory of the Department of Physics, University of Cape Town, South Africa. The experimental data were obtained automatically from ROYPROF profile algorithm synchronised with the automated process of the slow positron beam facility. The models, however, produce a slightly narrower range for the calculated S and W parameters, than those obtained experimentally.

5.4 Limitations of Study

In any case, the perceived limitation of this work lies in the limitation of Doppler-broadening slow positron studies to numerical characterisation of the S and W parameters for defect profiling. Three-dimensional structural defect studies are better off with Three-dimensional angular correlation of annihilation radiation (3D-ACAR). However, the high energy (>40keV) required for 3D-ACAR can only presently be obtained from a positromiun beam, which presently is very expensive to build, not to talk of its maintenance. This work was also limited by availability of experimental data for testing the models.

5.5 Recommendations for Further Studies

Having proposed and tested models for the calculation of S and W parameters of metals and semiconductors, the following recommendations are made for further studies:

i.) the model should be tested for other metals and semiconductors, and where possible, modifications should be made

ii.) a model should be developed to study positron diffusion in metals and semiconductors

iii.) a generalised code for structural characterisation of materials, based on positron annihilation technique, should be developed

iv.) the S and W parameters for positron annihilation in metals and semiconductors, should be studied using Monte Carlo process, and the results obtained, compared with the ones we obtained in this work.

REFERENCES

Alatalo M., Kauppinen H., Saarinen K., Puska M. J., Mäkinen J., Hautojärvi P. and Nieminen R. M. (1995). Identification of vacancy defects in compound semiconductors by core-electron annihilation: Application to InP. Physical Review B 51 (7): 4176-4185.

Alatalo M., Barbiellini B., Hakala M., Kauppinen H., Korhonen T., Puska M. J., Saarinen K., Hautojärvi P. and Nieminen R. M. (1996). Theoretical and experimental study of positron annihilation with core electrons in solids. Physical Review B 54 (4): 2397-2409.

Beling C. D., Fung S., Li Ming, Gong M. and Panda B. K. (1999). A theoretical search for possible high efficiency semiconductor–based field–assisted positron moderators. Applied Surface Science (N. H. Elsevier) 149: 253-259.

Börner F., Eichler S., Polity A., Krause-Rehberg R., Hammer R. and Jurisch M. (1999). Large-depth defect profiling in GaAs wafers after saw cutting. Applied Surface Science 149: 151-158.

Britton D. T., Rice-Evans P. C. and Evans J. H. (1985). Design of a low energy positron beam. Nuclear Instruments and Methods in Physics Research B12: 426-429.

Britton D. T. (1994). Time-dependent diffusion models of the annihilation of low energy positrons implanted in solids. Proceedings of the Royal Society of London A 445: 57-67.

Brusa R. S., Karwasz G. P., Tiengo N., Zecca A., Corni F., Tonini R. and Ottaviani G. (2000). Formation of vacancy clusters and cavities in He-implanted silicon studied by slow-positron annihilation spectroscopy. Physical Review B (The American Physical Society) 61 (15):10154-10166.

Coleman P. (2000). Positron Beams and their applications. World Scientific Publication, Singapore.

Dannefaer S., Bretagnon T., Foucaran A., Taliercio T. and Kerr D. (1995).Positron lifetime spectroscopy of n-type and p-type porous silicon. Thin Solid Films 55: 171-173.

Eichler S. and Krause-Rehberg R. (1999). Comparison of experimental and theoretical Doppler broadening line-shape parameters. Applied Surface Science 149: 227-233.

Eldrup M. (1995). Positron Methods for the Study of Defects in Bulk Materials. Journal de Physique IV C1: 93-109.

Eldrup M. and Singh B. N. (1997). Studies of defects and defect agglomerates by positron annihilation spectroscopy. Journal of Nuclear Materials (N. H. Elsevier) 251: 132-138.

Gebauer J., Krause-Rehberg R., Eichler S. and Börner F. (1999). Doppler broadening spectroscopy using the FAST-ComTec two-dimensional coincidence system: A case study. Applied Surface Science (N. H. Elsevier) 149: 110-115.

Ghosh V. J., Nielsen B., Kruseman A. C., Mijnarends P. E., van Veen A. and Lynn K. G. (1999). The effect of the detector resolution on the Doppler broadening measurements of both valence and core electron-positron annihilation. Applied Surface Science (N. H. Elsevier) 149: 234-237.

Gramsch E., Lynn K. G., Throwe J. and Kanazawa I. (1999). Positron diffusion in solid and liquid metals. Physical Review B (The American Physical Society) 59 (22): 14282-14301.

Hueβer H., Hugenschmidt C., Wider T. and Maier K. (1999). Slow positron beam facility for investigations of plastically deformed metals and surface crystallization of silica. Applied Surface Science (N. H. Elsevier) 149: 49-53.

Jain P. C., Lee S. K., Hozhabri N. and Sharma S. C. (1999). Phase transitions in physisorbed ethane investigated by positron-annihilation spectroscopy. Physical Review B (The American Physical Society) 60 (3): 2057-2063.

Krause-Rehberg R. and Leipner H. S. (1999). Positron Annihilation in Semiconductors: Defect Studies. Springer-Verlag.

Osiele M. O., Fuwape I. A. and Asaolu I. A. (2001). Models for calculating positron annihilation rates in solids.b Global Journal of Pure and Applied Sciences 7 (4): 637-640.

Puska M. J., Corbel C. and Nieminen R. M. (1990). Positron trapping in semiconductors. Physical Review B (The American Physical Society) 41 (14): 9980-9993.

Rice-Evans P., Saleh A. S. Nathwani M. Taylor J. W. and Foxon C. T. (1999). Positron studies of MBE-grown gallium nitride.Applied Surface Science 149: 165-169.

Saleh A. S., Taylor J. W. and Rice-Evans P. C. (1999). The ROYPROF program for analyzing positron profiling data obtained from variable energy beams. Applied Surface Science 149: 87-96.

Sato K., Takahashi Y, Uchiyama H., Kanazawa I., Tamura R., Kimura K., Komori F., Suzuki R., Ohdaira T. and Takeuchi S. (1999). Positron-annihilation studies of stable Al-based icosahedral quasicrystals. Physical Review B (The American Physical Society) 59 (10): 6712-6716.

Seeger A. and Britton D. T. (1999). Slowing-down and penetration of positrons in condensed matter. Applied Surface Science (N. H. Elsevier) 149: 287-303.

Stoeffl W., Asoka-Kumar P. and Howell R. (1999). The positron microprobe at LLNL. Appled Surface Science (N. H. Elsevier) 149: 1-6.

Uedono A., Mori K., Morishita N., Itoh H., Tanigawa S., Fujii S. and Shikata S. (1999). Annealing behaviours of defects in electron-irradiated diamond probed by positron annihilation. Journal of Physics: Condensed Matter (IOP Publishing) 11: 4925-4934.

Uedono A., Fujii S., Moriya T., Kawano T., Tanigawa S, Suzuki R., Ohdaira T.and Mikado T. (1997). Defects in the Ti/GaAs system probed by monoenergetic positron beams. Journal of Physics: Condensed Matter (IOP Publishing) 9: 6827-6835.

edono A., Watanabe M., Takasu S., Sabato T. and Tanigawa S. (2000). Positron annihilation in silicon in thermal equilibrium at high temperature. Journal of Physics: Condensed Matter (IOP Publishing) 12: 719-728.

n Huis M. A., van Veen A., Schut H., Falub C. V., Eijt S. W. H., Mijnarends P. E. and Kuriplach J. (2002). Positron confinement in embedded lithium nanoclusters. Physical Review B (The American Physical Society) 65 (8): 085416(1)-085416(11).

ang Z., Wang S. J., Chen Z. Q., Ma L. and Li S. Q. (2000). Defect Properties in Plastically Deformed p-GaAs Studied by Positron Lifetime Measurements. Physical State of Solids (a) 177: 341-348.